




RESEARCH ARTICLE

Journal of Ecology



Adaptive trait syndromes along multiple economic spectra define cold and warm adapted ecotypes in a widely distributed foundation tree species

Davis E. Blasini^{1,2}  | Dan F. Koepke² | Kevin C. Grady^{3,4} | Gerard J. Allan^{4,5}  | Catherine A. Gehring^{4,5} | Thomas G. Whitham^{4,5} | Samuel A. Cushman⁶ | Kevin R. Hultine² 

¹School of Life Sciences, Arizona State University, Tempe, AZ, USA; ²Department of Research, Conservation and Collections, Desert Botanical Garden, Phoenix, AZ, USA; ³School of Forestry, Northern Arizona University, Flagstaff, AZ, USA; ⁴Center for Adaptable Western Landscapes, Flagstaff, AZ, USA; ⁵Department of Biological Sciences, Northern Arizona University, Flagstaff, AZ, USA and ⁶U.S. Department of Agriculture, Forest Service, Rocky Mountain Research Station, Forest and Woodland Ecosystems Program, Flagstaff, AZ, USA

Correspondence

Davis E. Blasini

Email: dblasini@asu.edu

Funding information

National Science Foundation, Grant/Award Number: DEB-1340852, DEB-1340856 and MRI-DBI-1126840

Handling Editor: Giovanna Battipaglia

Abstract

1. The coordination of traits from individual organs to whole plants is under strong selection because of environmental constraints on resource acquisition and use. However, the tight coordination of traits may provide underlying mechanisms of how locally adapted plant populations can become maladapted because of climate change.
2. To better understand local adaptation in intraspecific trait coordination, we studied trait variability in the widely distributed foundation tree species, *Populus fremontii* using a common garden near the mid-elevational point of this species distribution. We examined 28 traits encompassing four spectra: phenology, leaf economic spectrum (LES), whole-tree architecture (Corner's Rule) and wood economic spectrum (WES).
3. Based on adaptive syndrome theory, we hypothesized that trait expression would be coordinated among and within trait spectra, reflecting local adaptation to either exposure to freeze-thaw conditions in genotypes sourced from high-elevation populations or exposure to extreme thermal stress in genotypes sourced from low-elevation populations.
4. High-elevation genotypes expressed traits within the phenology and WES that limit frost exposure and tissue damage. Specifically, genotypes sourced from high elevations had later mean budburst, earlier mean budset, higher wood densities, higher bark fractions and smaller xylem vessels than their low-elevation counterparts. Conversely, genotypes sourced from low elevations expressed traits within the LES that prioritized hydraulic efficiency and canopy thermal regulation to cope with extreme heat exposure, including 40% smaller leaf areas, 67% higher stomatal densities and 34% higher mean theoretical maximum stomatal conductance. Low-elevation genotypes also expressed a lower stomatal control over leaf water potentials that subsequently dropped to pressures that could induce hydraulic failure.

5. *Synthesis.* Our results suggest that *Populus fremontii* expresses a high degree of coordination across multiple trait spectra to adapt to local climate constraints on photosynthetic gas exchange, growth and survival. These results, therefore, increase our mechanistic understanding of local adaptation and the potential effects of climate change that in turn, improves our capacity to identify genotypes that are best suited for future restoration efforts.

KEYWORDS

Corner's Rule, experimental common garden, foliage phenology, leaf economic spectrum, Physiology, plant–climate interaction, wood economic spectrum, xylem anatomy

1 | INTRODUCTION

Functional trait expression in plants underlies their performance in relation to local environmental conditions (Chapin et al., 2011; Lambers et al., 2008). However, the coordination of traits across multiple scales from individual organs to whole plants has only recently been addressed in the study of organisms and communities across broad environmental gradients (Freschet et al., 2010; Kleyer & Minden, 2015; Messier et al., 2017; Reich, 2014; Reich et al., 2003; Rosas et al., 2019). Two classic examples of how trait variability relates to environmental gradients are captured in the leaf economic spectrum (LES) and in Corner's Rules (CR). While LES describes how leaf traits govern the acquisition and utilization of carbon and nutrients at various interspecific scales (Wright et al., 2004), CR defines the adaptive significance of whole-plant morphology (e.g. organ size), architecture (e.g. branching patterns) and function (e.g. hydraulics and biomechanics) across resource gradients (Lauri, 2019; Messier et al., 2017; Valladares et al., 2002). More recently, the 'world-wide fast-slow plant economic spectrum' and 'wood economic spectrum (WES)' have shown that the principles of LES and CR can be applied to other plant organs such as stems and roots (Chave et al., 2009; Reich, 2014).

The whole-plant economic spectrum provides a potentially robust integrative description of the coordination among traits and resource-fluxes within and among plants (Freschet et al., 2010; Reich, 2014). Accordingly, there are whole-plant or multi-organ coordinated trade-offs between the rate of resource acquisition and conservation that explain the performance of a plant in terms of growth and survival (Chave et al., 2009; Freschet et al., 2010; Reich, 2014). For example, plants with higher wood densities also often have more compact and smaller xylem vessels. Although higher wood densities often reflect lower maximum hydraulic conductivity, it provides greater mechanical and protective features that enhance survival when faced with environmental stress (Chave et al., 2009; Reich, 2014; Sperry & Sullivan, 1992). Conversely, plants with acquisitive or exploitative traits characteristically display higher maximum resource uptake and transport efficiency such as higher maximum hydraulic conductivity, higher photosynthetic capacity and higher growth rates at the risk of having reduced tolerance to environmental stress (Lambers & Poorter, 1992; Reich, 2014).

Studying the adaptive significance of coordinated traits along a broad climatic gradient is critical for predicting whether a specific population that is locally adapted to a narrow range of climate conditions will become maladapted under rapid climate shifts. Common gardens are a powerful tool for studying patterns of local adaptation to evaluate adaptive variation among populations in individual traits, and the coordination of multiple traits over broad climate gradients (Clausen et al., 1940; Cooper et al., 2019; de Villemereuil et al., 2016; Germino et al., 2019; Kawecki & Ebert, 2004; Mooney & Billings, 1961). Common gardens can eliminate the confounding effects of the corresponding environment, and thus uncover adaptive variation in trait expression among widely dispersed populations. However, common garden studies of long-lived woody plants can be challenging to implement, and consequently only a relatively small fraction of woody plant species have been critically evaluated within common garden studies.

Populus fremontii, Sarg. (Fremont cottonwood), is among the most dominant riparian tree species in the southwestern US and northern Mexico, and is an ideal species to evaluate adaptive trait syndromes for a number of reasons. First, *P. fremontii* is distributed across an extremely broad climate gradient that encompasses regular freezing temperatures in high-desert locations to extreme heat exposure in low-desert locations. Second, *P. fremontii* shares many morphological and ecological features with relatives within the genus that includes 29 species broadly distributed throughout North America, Africa, Asia and Europe (Eckenwalder, 1996). Third, like many species within the genus, *P. fremontii* is recognized as a foundation species that supports numerous communities through genetically based functional trait variation (Whitham et al., 2008). Finally, many *Populus* species, including *P. fremontii* has experienced a substantial decline in its historical distribution due to climate change and other environmental changes (Hultine & Bush, 2011; Hultine et al., 2010; Stromberg, 1993; Worrall et al., 2008, 2013; Zhou et al., 2020). Consequently, *P. fremontii* and other similar tree species are rapidly becoming maladapted to their local environmental conditions (Grady et al., 2011; Hultine, Allan, et al., 2020; Hultine, Froend, et al., 2020; Merritt & Leroy Poff, 2010).

There is evidence suggesting that climate change-driven maladaptation may vary among populations within the same species (Ikeda et al., 2014; O'Neill et al., 2008). For instance, populations

with certain physiological and morphological traits (e.g. high-water use efficiency, low SLA) may be better equipped to withstand drier and hotter conditions than other populations (Chapin et al., 2011; Lambers et al., 1998; Smith & Allen, 1996). This can be especially critical for *P. fremontii* because recent landscape genetic studies across the species entire geographical distribution have identified genetically distinct ecotypes that are distributed across geographically distinct ecoregions (Ikeda et al., 2017). These ecotypes occur within the Sonoran Desert region in southern Arizona and northern Mexico (Sonora Desert, SD), the Mogollon Rim in Northern Arizona (Mogollon Rim, MR), the Colorado Plateau and northern Great Basin region from southern Utah to western Colorado (Utah High Plateaus, UHP), and the Central Valley and coastal regions of California (California Central Valley, CCV; Cushman et al., 2014; Ikeda et al., 2014) (H. M. Bothwell and G. J. Allan, unpubl. data). Although previous common garden experiments have uncovered intraspecific trait variation in *P. fremontii* (Grady et al., 2011, 2013) these studies have mainly investigated adaptive variation of leaf traits measured in populations sourced exclusively from the SD ecotype that only represent the warmest edge of the climatic gradient of this species' distribution. Thus, the adaptive trait coordination among multiple trait spectrums, and their potential significance to potential maladaptation to climate shifts remain an open question.

In this study, we used an experimental common garden located near the thermal and elevational mid-point of *P. fremontii*'s distribution (988 m; Figure 1; Table 1) to study trait variability in relation to elevation and the mean annual temperature (MAT) transfer distance, defined as the MAT of the source population location subtracted from the MAT of the common garden location (Grady et al., 2011). We studied contrasts in morpho-physiological coordination in functional trait expression among eight *P. fremontii* populations spanning two ecotypes (SD and MR) and an approximate 12°C mean annual temperature gradient (Wang et al., 2012). We analysed four trait spectra including: foliage phenology (spring budburst and budset), trait variability across a leaf economic spectrum, including petiole traits (LES), trait variability across a wood and xylem economic spectrum (WES), and trait variability in above-ground architecture, including traits related to Corner's Rule (CR; Cornelissen, 1999; Corner, 1949; Lauri, 2019; Messier et al., 2017). Combined, these trait spectra represent coordinated strategies at multi-organ levels for coping with climate stress exposure from intense freezing events at higher latitudes and elevations to episodic heat waves at lower latitudes and elevations.

We hypothesized that the combined intraspecific coordination of traits across all trait spectra reflect local adaptation to both the extreme high temperatures in the SD ecotype as well

FIGURE 1 Location of eight source population sites of *Populus fremontii* and the Agua Fria common garden locations (Fremont cottonwood leaf icon). Light blue points denote populations coming from the Mogollon Rim ecotype while the pink points indicate populations coming from the Sonoran Desert ecotype (S.E. Fick and R.J. Hijmans, 2017. Worldclim 2: New 1-km spatial resolution climate surfaces for global land areas. International Journal of Climatology, <http://worldclim.org/version2>). QGIS Development Team (2020). QGIS Geographic Information System. Open Source Geospatial Foundation Project. <http://qgis.osgeo.org>

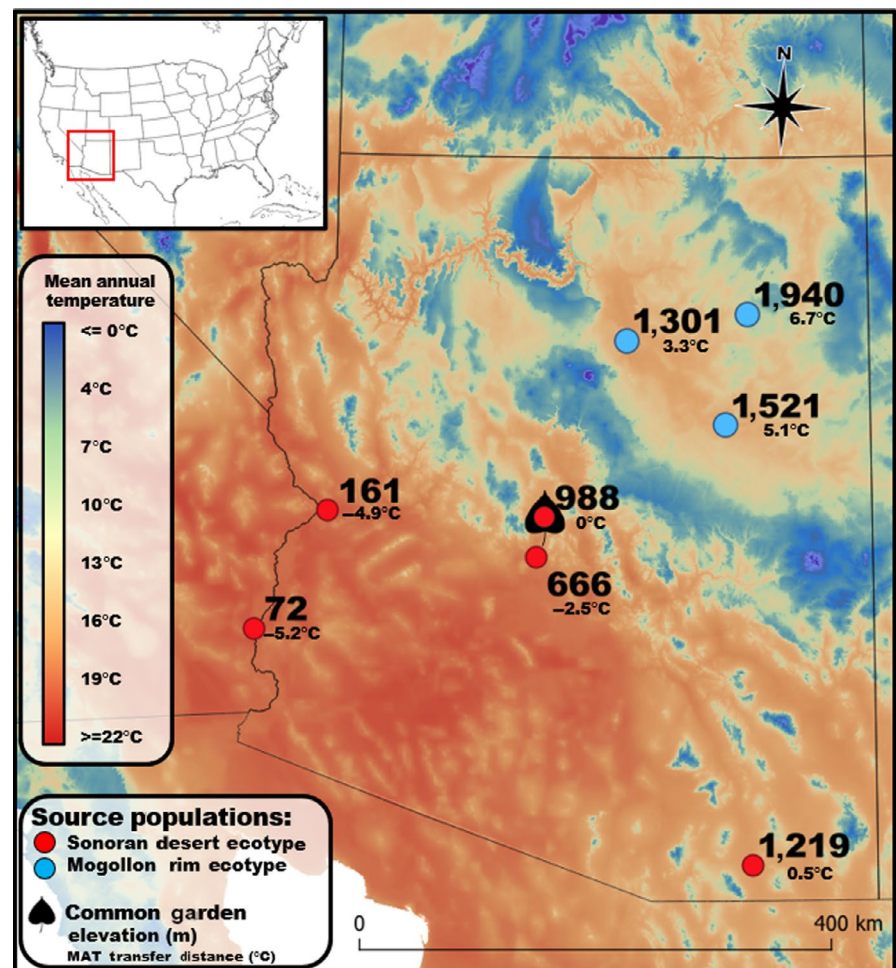


TABLE 1 Climatic variables of the eight provenances and their corresponding two ecotypes studied at the Agua Fria National Monument common garden. Climatic characteristics include mean annual temperature (MAT), mean warmest monthly temperature (MWMT) and mean coldest monthly temperature (MCMT). Transfer distances for MAT (MAT of the garden minus MAT of the provenance), MWMT and MCMT. The population CAFAUG is located near the common garden and thus has a transfer distance of zero

Population	Elevation (m)	Latitude	Longitude	MAT (°C)	MWMT (°C)	MCMT (°C)	MAT (°C) Transfer	MWMT (°C) Transfer	MCMT (°C) Transfer
MR ecotype									
KKHOPI	1,940	35.8115	-110.18038	10.7	23.0	-1.3	6.7	5.7	9.1
JLAJAK	1,521	34.9613	-110.38956	12.3	25.3	-0.7	5.1	3.4	8.5
CLFLCR	1,301	35.6088	-111.31369	14.1	27.2	0.8	3.3	1.5	7.0
SD ecotype									
TSZSAN	1,212	31.4382	-110.76260	16.9	26.2	8	0.5	2.5	-0.2
CAFAUG	988	34.2338	-111.04478	17.4	28.7	7.8	0	0	0
NRVNEW	666	33.9540	-112.13526	19.9	31.4	10.0	-2.5	-2.7	-2.2
LBWBIL	161	34.2761	-114.05856	22.3	34.6	10.9	-4.9	-5.9	-3.1
CCRCOL	72	33.3621	-114.69856	22.6	33.9	12.2	-5.2	-5.2	-4.4

as exposure to freeze-thaw events in the MR ecotype. We argue that this hypothesis can be generalized as the economic spectrum similarity rule in which plants with functionally related traits at low trait level (epidermal and vascular tissue) scale up to functionally related traits at higher (organ to whole-tree) trait level. Because phenology, leaf, whole-tree architecture and wood traits are, in part, genetically based (Bailey et al., 2004; Barbour et al., 2015; Cooper et al., 2019; Preston et al., 2006), our findings provide a genetic mechanism for the potential evolution of a general adaptive plant stress syndrome in which many traits would be accumulated in each ecotype to best survive their specific environments (Rueda et al., 2018). The same logic applies to our proposed economic spectrum similarity rule. Tests of this hypothesis are reflected in the following sub hypotheses. (a) At the leaf level, warm-adapted SD ecotype trees should possess a suite of traits that maximize stomatal conductance and transpirational cooling while reducing foliar exposure to radiation and thermal load. MR ecotype trees, on the other hand, should possess characteristics reflecting shorter growing season duration and a more conservative hydraulic strategy to cope with episodic freezing events. (b) Above-ground architecture in SD ecotype trees should be constructed to prioritize leaf water supply relative to demand while the MR ecotype trees should maximize leaf sun exposure over their shorter growing season. (c) At the wood trait level, intraspecific differences in xylem hydraulic traits should reflect a trade-off between maximizing hydraulic efficiency in the SD ecotype trees to reducing vulnerability to cavitation during freeze-thaw cycles in MR ecotype trees by constructing smaller and hydraulically less efficient xylem vessels. 4. In addition to expecting differences in these traits across levels of organization between ecotypes, we also expected finer levels of local adaptation within ecotypes. Information derived from this research will help shape our understanding of local adaptation related to climate-induced

resource limitation in *P. fremontii*, and other widely distributed *Populus* species threatened with climate change.

2 | MATERIALS AND METHODS

2.1 | Study site and plant material

An experimental common garden was established in October 2014 with ~4,100 propagated cuttings from 16 populations that represent the entire climatic gradient of *P. fremontii* within the state of Arizona. The garden is located on a 1.2 Ha portion of historic cropland within the Agua Fria National Monument (N 34.2567, -112.0661, elevation 988 m). To avoid using clones within each population, all cuttings were collected randomly from trees at least 20 m apart during the 2013–2014 winter. Individual cuttings were grown in pots in the Northern Arizona University greenhouse for 4 months and then transplanted to the common garden when saplings were approximately 0.3 m in height. During the growing season, the garden was drip irrigated with approximately 20 litres per tree, two to three times per week. In this study, 10 genotypes were randomly selected from five Arizona Sonoran Desert (SD) ecotype populations and from three Mogollon Rim (MR) ecotype populations ($n = 80$ total ecotypes). Climatic variables from each sampling location were obtained using the platform ClimateWNA (Wang et al., 2012; Table 1). For climatic data regarding number of days with temperatures above/below freezing and above 40°C, we used modelled estimates of temperature from PRISM data. Copyright © <2020>, PRISM Climate Group, Oregon State University, <http://prism.oregonstate.edu>. The eight populations were chosen because they collectively represent the broadest possible range in mean annual temperature from 10.7 to 22.6°C, and an elevation gradient from 72 to 1,940 m (Table 1; Figure 1) Likewise, the eight populations selected for this study had a mean annual temperature transfer distance to the common garden

of 3.3 to 6.7°C in the MR populations and a −5.2 to 5.0°C in the SD populations (Table 1).

2.2 | Measured traits

Between the 2016–2018 growing seasons, we measured 28 traits on 48–80 genotypes representing the eight populations described above. These traits were categorized according to their respective trait spectrum which include foliage phenology, LES, CR and WES (Table 2).

Foliage phenology—From February 13 to May 9 and from October 4 to 30 of 2017, we evaluated phenophase status on spring budburst and fall budset every 15 days following the USA National

Phenology Network protocol (Denny et al., 2014). Repeated observational assessment of presence or absence of the two phenological events of interest were monitored in all eight populations on ($n = 10$ genotypes). We recorded the date of the emergence of new leaves, budburst status, per individual ecotypes as zero, <50 and >50 budburst occurrences. For budset, we noted the dates of the appearance of the first 20 terminal buds in each genotype.

2.3 | LES traits

Stomatal anatomy—In 2016, fully expanded leaves were collected from outer leaves on the south facing side of mid-canopy height to

TABLE 2 Hypothesized correlations between the set of functional traits studied in this research and the two ecotypes (Sonoran Desert ecotype and the Mogollon Rim ecotype) present in the Agua Fria National Monument common garden

	Acronym	Unit	SD ecotype	MR ecotype
Phenology				
Spring budburst	BB	Day of the year	Early	Late
Fall budset	BS	Day of the year	Late	Early
Leaf traits				
Individual leaf area	A_{il}	cm ²	Small	Large
SLA	SLA	cm ² /g	High	Low
Stomatal density	D_{stom}	#Stomata/mm ²	High	Low
Stomatal size	S_{stom}	μm ²	Small	Large
Theoretical maximum stomatal conductance	G_{smax}	mmol m ⁻² s ⁻¹	High	Low
Petiole area	A_p	mm ²	Small	Large
Petiole flatness	L_{pf}	mm ² /mm ²	Low	High
Petiole lumen area	A_{pl}	μm ²	Large	Small
Petiole hydraulic mean diameter	Hd_p	μm	Large	Small
Petiole lumen fraction	F_{pl}	μm ² /μm ²	Large	Small
Petiole vessel density	D_{pv}	# vessel/mm ²	High	Low
Petiole theoretical hydraulic conductivity	K_p	mg m Mpa ⁻¹ s ⁻¹	High	Low
Leaf theoretical hydraulic conductivity	K_l	mg m ⁻¹ Mpa ⁻¹ s ⁻¹	High	Low
Architecture traits				
Whole-tree leaf area	A_l	m ²	Small	Large
Tree height	H	m	Tall	Short
Canopy area	A_c	m ²	Small	Large
Sapwood to leaf area	$A_s:A_l$	cm ² /cm ²	Large	Small
Leaf area index	LAI	m ² /m ²	High	Low
Wood traits				
Specific stem density	D_{stem}	g/cm ³	Low	High
Bark %	F_b	%	Low	High
Stem lumen area	A_{sl}	μm ²	Large	Small
Stem hydraulic mean diameter	Hd_s	μm	Large	Small
Stem lumen fraction	F_{sl}	μm ² /μm ²	Large	Small
Stem vessel density	D_{sv}	# vessel/mm ²	High	Low
Pre-dawn water potential	Ψ_{pd}	Mpa	Same	Same
Mid-day water potential	Ψ_{md}	MPa	Low	High

assess stomatal density, length, width and area. Following the nail polish impression method (Hilu & Randall, 1984), 160 impressions on both the abaxial and adaxial sides of the leaves ($n = 640$ images) were obtained to be observed under an Olympus CX41light microscope and images were taken with a Moticam Pro 282A camera (Motic). Stomatal density was estimated as the number of stomata in eighty 0.59 mm^2 digital images at $10\times$ magnification. Stomatal sizes (length \times width) were estimated on 800 stomata from digital images at $40\times$ magnification ($n = 100$ per population) using an open-source imaging program, ImageJ (<https://imagej.nih.gov/ij/>). Maximum theoretical stomatal conductance to water vapour ($\text{mmol m}^{-2} \text{ s}^{-1}$) was calculated from Franks and Farquhar (2001):

$$G_{\text{smax}} = \frac{dw \times D_s \times a_{\text{max}}}{v \left(1 + \frac{\pi}{2} \sqrt{\frac{a_{\text{max}}}{\pi}} \right)}, \quad (1)$$

where dw is the diffusivity of water in air ($2.43 \times 10^{-5} \text{ m}^2/\text{s}$), v is the molar volume of air ($0.024 \text{ m}^3/\text{mol}$; Jones, 2013), D_s is the stomatal density, a_{max} is the maximum area of the open stomatal pore, approximated as $\pi(p/2)^2$, where p is stomatal pore length, assumed to be stomatal length divided by two (Franks & Farquhar, 2007).

Leaf traits—SLA was calculated as the one-sided area of a fresh leaf, divided by its oven-dry mass (Wright & Westoby, 2002). SLA was measured in June, July and September 2017. A subset of 12–20 collected leaves per tree were scanned with a high-resolution computer scanner, and one-sided leaf area was measured with ImageJ. The scanned leaves were then oven-dried for 72 hr at 75°C and weighed to calculate SLA (cm^2/g). Individual leaf area (A_{il}) was derived from the average individual leaf area from these measurements (Ackerly et al., 2002).

Petiole traits—In September 2017, three to four leaves located at the mid-canopy level and south-facing side were collected from six trees per population to study petiole traits. Leaf samples were stored in a cooler at approximately $7\text{--}10^\circ\text{C}$ and transported to the Imaging and Histology Core Facility at Northern Arizona University. Individual petioles were cut with a razor blade and their mid-portions were sectioned to fit within embedding cassettes ($28.5 \times 41.0 \times 6.7 \text{ mm}$). The samples were prepped using an automated fixation and paraffin embedding process. Specifically, the samples were fixed with formalin, dehydrated with increasing concentrations of undenatured alcohol, cleared with xylene to then be infiltrated with paraffin, and then embedded into the cassette. Cassette blocks were then sliced into transverse sections approximately $5\text{--}10 \mu\text{m}$ thick with a microtome and moulded onto positively charged slides, deparaffinized with xylene and rehydrated with decreasing concentrations of undenatured alcohol until rinsing with only DI water, and then stained with 0.1% toluidine blue. Images were produced on a digital light microscope that were subsequently analysed using ImageJ. Several petiole characteristics were recorded, including the length, width and area of the entire petiole (A_{p}). Additionally, we measured petiole xylem vessel diameter (d), vessel density (D_{pv}), mean and total lumen area of all of the vessels contained in the petiole (A_{pl}), the hydraulically

weighted mean vessel diameter (Hd_{p}) was calculated as $\Sigma d^5 / \Sigma d^4$ (Scholz et al., 2013; Sperry & Saliendra, 1994). Petiole flatness (L_{pf})—a distinct characteristic of *Populus* species—was quantified from the petiole width to length ratio at the mid-rib of the petiole (Lindtke et al., 2013). The petiole lumen fraction (F_{pl}) was calculated as total A_{pl} per petiole transverse area (A_{p}) at the mid-rib.

Mean petiole theoretical hydraulic conductivity (K_{p} ; $\text{mg m MPa}^{-1} \text{ s}^{-1}$) was calculated from total petiole vessel lumen diameter using the Hagen–Poiseuille equation (Eguchi et al., 2008; Nobel, 2009; Tyree & Zimmermann, 2002):

$$K_{\text{p}} = \Sigma \frac{d_i^4 \pi \rho}{128 \eta_w}, \quad (2)$$

where d_i is the diameter of a single vessel (m), ρ is water density at 25°C (998 kg/m^3) and η_w is viscosity of water at 25°C ($8.9 \times 10^{-10} \text{ MPa s}$; Eguchi et al., 2008).

Theoretical hydraulic conductivity per unit leaf area (K_{l} , $\text{mg m}^{-1} \text{ s}^{-1} \text{ MPa}^{-1}$; Sack et al., 2003; Sack & Frole, 2006), was calculated as:

$$K_{\text{l}} = \Sigma \frac{K_{\text{p}}}{A_{\text{il}}}, \quad (3)$$

where A_{il} is the area of the leaf (m^2) attached to the petiole and K_{p} is the mean petiole theoretical hydraulic conductivity. Additionally, we estimated differences in water use strategies at the population and ecotype levels by dividing leaf area normalized theoretical hydraulic conductivity of the petiole (K_{l} , $\text{mg m}^{-1} \text{ s}^{-1} \text{ MPa}^{-1}$) by G_{smax} .

2.4 | CR traits

In July 2017, we estimated whole-tree leaf area (A_{t}) and sapwood area (A_{s}) using population-specific allometric relationships between stem diameter to leaf area through a branch summation approach (Jones et al., 2015; Kenefic & Seymour, 1999). Thus, whole-tree leaf area was estimated per branch by multiplying the mass of all leaves by their respective SLA. Canopy diameters (4–8 measurements per tree) and their respective canopy areas together with whole-tree height (H) were measured five times during the 2016 and 2017 growing seasons with a telescoping measuring pole. Canopy area (A_{c}) was determined using the ellipse equation, πab , where a is the mean radius of longest canopy axes and b is the radius of two perpendicular canopy axes (Ansley et al., 2012). Leaf area index (LAI) was estimated by the equation from (Hultine et al., 2013):

$$\text{LAI} = \frac{A_{\text{t}}}{A_{\text{c}}}. \quad (4)$$

2.5 | WES traits

In May to June 2018, we collected 1-year-old stem samples to measure wood and xylem traits. We collected branch cuttings approximately

1-cm diameter and cut the segment to a length of 30 cm. The segments were placed into a plastic bag with a moist paper towel and kept in a cooler until being transferred to a lab refrigerator kept at 4°C. Specific wood density (D_{stem}) was determined using Archimedes' principle of water displacement (Cornelissen et al., 2003; Hacke et al., 2000; Preston et al., 2006). The outer bark was removed from a 1 cm diameter stem segment. The segments were cut to a length of approximately 15 cm with no obvious side branches and total stem volume with the bark was measured. Specifically, a graduated cylinder with water was tared on a scale with 0.01-g accuracy, and the segment was submerged just below the meniscus; the weight was recorded and converted to volume. After the whole stem volume was initially measured, the bark was removed and the sapwood volume was measured using the same method. The samples were then oven-dried at 70°C for 48 hr, and a dry weight was recorded. D_{stem} was determined as the ratio of dry weight to volume displaced of the sapwood. The whole stem volume was measured to assess the stem bark fraction (F_b).

Xylem vessel area was determined from the 1 cm diameter segments used for density by first removing 2 cm length segments to mount in a GSL1 sledge microtome (Gärtner et al., 2014). The samples were moistened with a Strasburger solution (Eilmann et al., 2011) before being shaved into 100–150 μm slices. The fresh cut slices were transferred to a dye solution of 0.1% toluidine blue for 1–2 min (Sridharan & Shankar, 2012) before being dehydrated by increasing concentrations of undenatured alcohol (50%, 70%, 95% and 99.5% EtOH; KOPTEC 200 proof, VWR; Buesa & Peshkov, 2009). At the end of this process, we used the synthetic mounting medium Permunt (Mayr et al., 2014; Ravikumar et al., 2014) to embed the samples. Slides were photographed with a Moticam Pro 282A camera (Motic, Richmond, BC, Canada) mounted to an Olympus CX41light microscope. The region of interest included a subset of the previous year's growth ring to include both the early wood and late wood. Vessel lumen area was measured using ImageJ software, and individual images were stitched together (Preibisch et al., 2009) to analyse xylem vessels of the entire growth year. The number of vessels measured per genotype ranged from 153 to 941 (mean = 460). From the images we quantified mean stem lumen area (A_{sl}), mean stem hydraulic diameter (Hd_s) and stem vessel density (D_{sv}). Stem lumen fraction (F_{sl}) was calculated as the total A_{sl} per D_{sv} .

Water potential - Monthly measurements of leaf water potential (Ψ) were taken from June to October of 2017 using the Scholander pressure chamber (Cochard et al., 2001; Scholander et al., 1965). Predawn and midday Ψ measurements were taken to assess possible differences in water potential gradients at the population and ecotype levels. A single shoot tip from each of the 64 trees was cut with a sharp razor blade to measure water potential at predawn (Ψ_{pd}) between 03:00 and 05:00 hr, and at midday (Ψ_{md}) between 11:00 and 13:00 hr.

2.6 | Statistical analysis

All statistical analyses were conducted in R version 3.6.2 (R Core Team, 2019). Prior to analysing the data, we examined whether

each variable met the assumptions of normality and homogeneity of variance, using a Shapiro and Barlett test. When the data were not normally distributed, they were normalized by log10, square root or box-cox transformations. Once the basic requirements were met, functional traits were analysed statistically using a linear regression with provenance elevation as the predictor and traits as the responses. We also used analysis of variance (ANOVA) to analyse differences among populations. When a trait showed significant variation, we used a Tukey's HSD post-hoc test to detect differences at the elevation level (Sokal & Rohlf, 1995). Trait contrasts at the ecotype level were analysed using a student's *t* test. Ecotype differences in traits measured several times during the growing season (A_{il} , SLA, A_c , H and Ψ_{pd} , Ψ_{md}) were analysed by individual mixed-model repeated measures ANOVA (type III with Satterthwaite's method) in the lmer R package (Bates et al., 2015; Kuznetsova et al., 2017). In this test, individual traits were represented as response variables while the ecotype and month were treated as fixed effects with two and three levels, respectively. Individual genotype nested within ecotype was the random effect.

We conducted separated principal component analyses (PCAs) on the three trait spectra (leaf, architecture and wood) and all traits pooled together using the factoextra and FactoMineR packages (Kassambara & Mundt, 2017; Lê et al., 2008). Because G_{max} is autocorrelated with D_{stem} and S_{stem} , it was excluded from these analyses. Thus, we simultaneously assessed what traits explained most of the variation within each trait spectrum and among all the remaining 27 *P. fremontii* traits together. For each PCA analysis, the variables showing the highest loading in each PCA were selected as indicators of local climatic adaptability. We initially determined the number of meaningful PCA axes using the Kaiser criterion. This criterion recommends using axes with eigenvalues above 1.0 exclusively. However, because the Kaiser criterion is not recommended to be used as the only cut-off criterion for estimating the number of factors (Grossman et al., 1991; Jackson, 1993; Peres-Neto et al., 2005), we also used the Broken Stick Model in the vegan and biodiversity R package to determine significant components. This model randomly divided a stick of components into the same number of elements found in the PCA axis. Then, these elements were rearranged in decreasing order according to their length to be compared to the eigenvalues. Axes with larger eigenvalues than their corresponding stick of components were considered significant (Borcard et al., 2011).

In each principal component graph (biplot), trait representation was based on the magnitude of the correlation (loadings) between traits and the given principal component. Thus, in each biplot, traits were represented as vectors with a length and direction indicating the strength and trend of a given trait's relationship among other traits. Specific location of the vector in the biplot indicates the positive or negative impact that a trait has on each of the two components x-axis, first component (PC1) and y-axis, second component (PC2). Additionally, to assess the relationship between the two ecotypes and the traits distribution in every PCA biplot, we constructed two 95% confidence ellipses based on

the PCA scores of each of the two ecotype means. Subsequently, linear regressions between significant principal components and elevation of source populations were constructed. Additionally, we performed *t* tests and ANOVA Tukey's HSD tests to assess significant differences in PC axes scores at ecotype and population levels. Because PC scores mainly described dominant traits in each axis, we evaluated population differences in all traits included in each PCA simultaneously by using a permutational multivariate analysis of variance (PERMANOVA; (Anderson, 2001) in the vegan R package. Population differences in all 27 traits PCA were further analysed with pairwise comparisons using permutation MANOVAs on a Pillai test and distance matrix in the VEGAN and RVAIDEMOIRE R packages.

Redundancy Analysis (RDA; Borcard et al., 2011) was used to determine how environmental (e.g. provenance latitude, longitude, mean annual precipitation, MAT transfer distance and ecotype) and genetic (e.g. ecotype) descriptors influence multi-spectra trait variance in *P. fremontii*. We also used forward stepwise selection of descriptor variables to determine the significance of each variable to the RDA. Forward selection determines the successive contribution of each descriptor to explaining trait variation and adds only those variables with significant contribution.

3 | RESULTS

3.1 | Foliage phenology

Consistent with our hypothesis of local adaptation to extreme high summer temperatures in the SD ecotype and early spring and fall freeze-thaw exposure in the MR ecotype, we found large differences in foliage phenology between these two groups. Thus, we found that budburst of the SD ecotype occurred on average 46 days earlier than the MR ecotype ($t = 15.65$, $df = 78$, $p < 0.001$, Table 3; Figure 2a). Similarly, on average budset occurred 13 days later in the SD ecotype compared to the MR ecotype ($t = 8.63$, $df = 78$, $p < 0.001$, Table 3; Figure 2b).

3.2 | Leaf economic spectrum traits

We found remarkable differences in leaf structural traits between the extreme hot adapted SD ecotype and the cold-adapted MR ecotype. Specifically, we found that the MR ecotype had 30% larger leaves ($t = 8.98$, $df = 78$, $p < 0.001$, Table 3) while SLA in the SD ecotype was on average 22% higher than the MR ecotype ($t = -8.42$, $df = 78$, $p < 0.001$, Table 3). Repeated measures analysis showed that A_{ij} increased ($F = 126.4$, $df = 2$, $p < 0.001$, Table S1) and SLA decreased ($F = 70.9$, $df = 1$, $p < 0.001$, Table S1) over the course of the growing season. Likewise, there was a significant interaction between time of year and ecotype in both A_{ij} ($F = 15.8$, $df = 1$, $p < 0.001$, Table S1) and SLA ($F = 6.3$, $df = 1$, $p < 0.01$, Table S1), indicating that differences between ecotypes depended on the time

TABLE 3 Results of mean \pm standard density ($n = 48$ to 80) comparison of *Populus fremontii* traits at ecotypes level [Arizona Sonoran Desert (SD) and the Mogollon Rim (MR)] in the Agua Fria National Monument common garden. Abbreviations for each parameter are shown in Table 2. Bold values indicate statistical significance

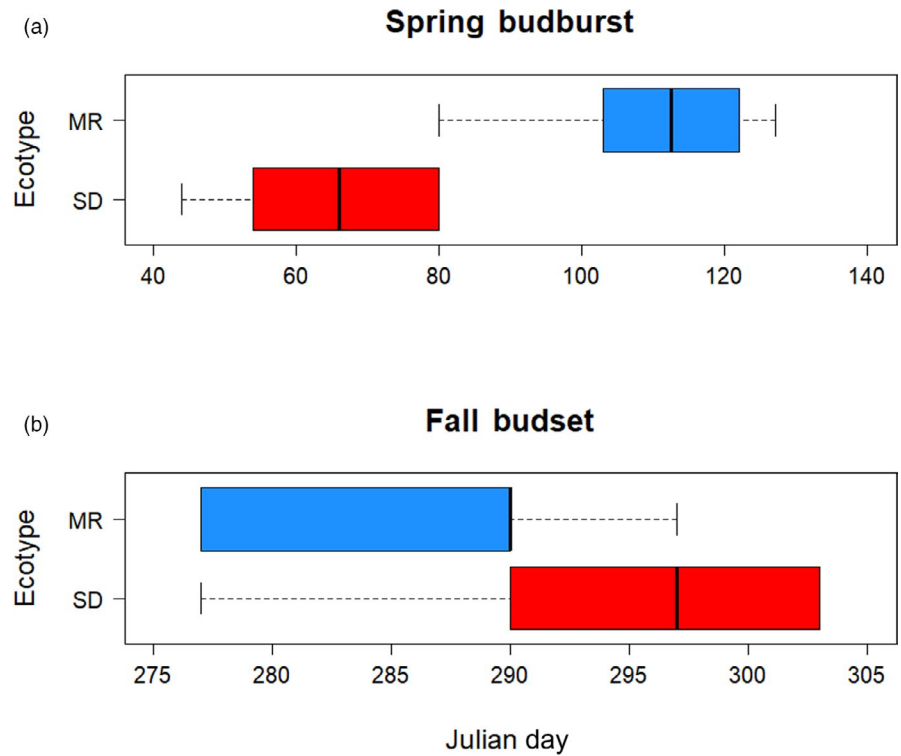
	t value	df	SD ecotype	MR ecotype
Phenology				
BB	-15.65***	78	65 \pm 11	111 \pm 14
BS	8.63***	78	297 \pm 6	284 \pm 7
Leaf spectrum				
A_{ij}	8.98***	78	18 \pm 5.25	30 \pm 6.81
SLA	-8.42***	78	121 \pm 11.9	99 \pm 9.64
D_{stom}	12.81***	77.6	430 \pm 73	258 \pm 47
S_{stom}	14.22***	78	250 \pm 34	394 \pm 58
G_{smax}	9.24***	77.1	1.25 \pm 0.18	0.93 \pm 0.12
A_p	-4.64***	46	1.04 \pm 0.48	1.69 \pm 0.43
L_{pf}	-3.25**	46	1.39 \pm 0.23	1.59 \pm 0.16
A_{pl}	-0.84	45.9	91.85 \pm 32	98.14 \pm 20
Hd_p	-1.43	38.5	23.4 \pm 3.1	24.7 \pm 2.9
F_{pl}	0.09	46	0.06 \pm 0.02	0.05 \pm 0.02
D_{pv}	1.09	46	677 \pm 354	575 \pm 232
K_p	-4.81***	46	7e-07 \pm 4e-07	1e-06 \pm 4e-07
K_l	-0.62	46	3e-04 \pm 1e-04	3e-04 \pm 9e-05
Architecture spectrum				
A_l	-2.26*	62	7.52 \pm 2.63	9.03 \pm 2.55
H	2.34*	78	3.08 \pm 0.49	2.84 \pm 0.36
A_c	4.02***	46.8	2.16 \pm 0.56	2.82 \pm 0.78
$A_s:A_l$	10.9***	43.5	3.56 \pm 0.55	2.58 \pm 0.10
LAI	0.68	59.3	3.61 \pm 1.73	3.36 \pm 1.27
Wood spectrum				
D_{stem}	-4.06***	46	0.41 \pm 0.03	0.44 \pm 0.03
F_b	-5.91***	46	0.29 \pm 0.06	0.39 \pm 0.06
A_{sl}	1.88.	46	779 \pm 192	679 \pm 153
Hd_s	2.28*	46	40.4 \pm 4	37.6 \pm 4
F_{sl}	2.66*	46	0.23 \pm 0.04	0.20 \pm 0.05
D_{sv}	0.24	46	318 \pm 78.2	313 \pm 85.1
Ψ_{pd}	-0.56	46	-0.46 \pm 0.04	-0.45 \pm 0.08
Ψ_{md}	-4.82***	46	-1.58 \pm 0.14	-1.38 \pm 0.13

Note: Signif. codes: ***0.001; **0.01; *0.05; .0.1.

of year and therefore might have different adaptive responses to seasonal conditions.

From June to September, we found a more pronounced increase in leaf sizes in the MR ecotype (66%) than the SD ecotype (46%). Over the same time, the SD ecotype displayed similar SLA values while the MR ecotype exhibited a 17% decrease (Table S1). Combined, the higher A_{ij} and lower SLA results suggest that the MR leaves have higher construction costs and longer lifespans than the SD leaves.

FIGURE 2 Box and whisker plots showing the median, 25th and 75th percentiles (boxes) and the 10th and 90th percentiles (error bars) of (a) spring budburst and (b) fall budset of the Sonoran Desert and Mogollon Rim ecotypes. Ecotype phenology was measured at the beginning and end of the 2017 growing season (Budburst: $t = -15.65$, $df = 78$, $p < 0.001$; Budset: $t = 5.02$, $df = 78$, $p < 0.001$)



Stomatal traits supported our hypothesis regarding selection for transpirational cooling in genotypes sourced from the SD region. Stomata in the SD ecotype were on average 37% smaller ($t = -14.22$, $df = 78$, $p < 0.001$, Table 3) but mean stomatal densities of the SD ecotype were 40% higher ($t = 12.81$, $df = 77.6$, $p < 0.001$, Table 3). The higher stomatal densities yielded a 34% higher G_{smax} in the SD ecotype ($t = 9.24$, $df = 77.1$, $p < 0.001$, Table 3), despite having smaller mean stomatal size.

Differences in leaf structure were accompanied by differences in petiole structure. The MR ecotypes had on average 63% larger petioles ($t = -4.64$, $df = 46$, $p < 0.001$, Table 3) that were 13% more elliptical (i.e. flatter) than the SD ecotypes ($t = -3.25$, $df = 46$, $p < 0.001$, Table 3). Conversely, none of the xylem vessel traits of the petioles differed between SD and MR ecotypes (Table 3). However, calculated petiole hydraulic conductivity was 80% higher ($t = -4.81$, $df = 46$, $p < 0.001$, Table 3) in the MR ecotypes, reflecting their larger petiole sizes and larger total lumen area compared to the SD ecotypes. Despite the higher K_p in the MR ecotype, the larger leaves in this ecotype resulted in K_l being similar between the two ecotypes (Table 3).

To better understand leaf functional variation in water supply versus demand in relation to climate, we analysed petiole theoretical K_p , K_l and G_{smax} in relation to source population MAT transfer distance. Theoretical K_p increased with elevation and positive MAT transfer distance ($R^2 = 0.31$, $F = 17.0$, $p < 0.001$, Figure 3a), although MAT transfer distance did not have a significant effect on K_l (Figure 3b). On the other hand, G_{smax} decreased with positive MAT transfer distance ($R^2 = 0.41$, $F = 27.9$, $p < 0.001$, Figure 3c) with the regression explaining 41% of the variation. We found that the ratio between leaf-level water supply (K_l) and the leaf-level demand

(G_{smax}) increased moderately with positive MAT transfer distance ($R^2 = 0.15$, $F = 7.47$, $p < 0.01$, Figure 3d), indicating that the low elevation (negative MAT transfer distance) genotypes may take on a riskier hydraulic strategy regarding the supply of water to the leaves relative to demand.

According to the Broken-Stick Model (Borcard et al., 2011), only the first two principal components significantly explained the variance within the leaf trait spectrum in *P. fremontii*. Together, these two principal components accounted for 55.7% of the variance. The first principal component axis, PC1 (accounting for 37.1% of the variance) showed a significant positive relationship with S_{stom} , A_{il} , A_p , K_p , L_{pf} , K_l , Hd_p , A_{pl} while showing opposite trends with D_{stom} , SLA and D_{pv} (Figure 4). The second axis, PC2 (which explained 18.6% of the variance) displayed significant positive correlations with SLA, A_{pl} , Hd_p and K_l and negative correlations with D_{pv} , F_{pl} , A_{il} and S_{stom} (Figure 4). Thus, the MR ecotype 95% confidence ellipse was found in the positive half of PC1 axis encompassing A_{il} , S_{stom} , K_p , A_p and L_{pf} trait vectors. The SD ecotype displayed a larger 95% confidence ellipse mainly located in the negative side of the PC1 axis (Figure 4). Accordingly, D_{stom} , SLA, D_{pv} , A_{pl} and K_l traits were found within this SD ecotype ellipse. Simultaneously, PC1 and PC2 displayed positive and negative significant relationships with the *P. fremontii* climatic range ($R^2 = 0.51$, $p < 0.001$, $R^2 = 0.14$, $p < 0.01$; Figure S1). We found PC1 and PC2 scores significantly differed between the two ecotypes ($t = -10.2$, $df = 46$, $p < 0.001$; $t = 3.21$, $df = 45.3$, $p < 0.01$). ANOVA and Tukey's HSD detected that the three populations with the negative MAT transfer distances displayed significantly lower PC1 scores than the three highest elevation populations with the most positive MAT transfer distances (Figure S1). Simultaneous evaluation of all leaf traits through PERMANOVA and pairwise

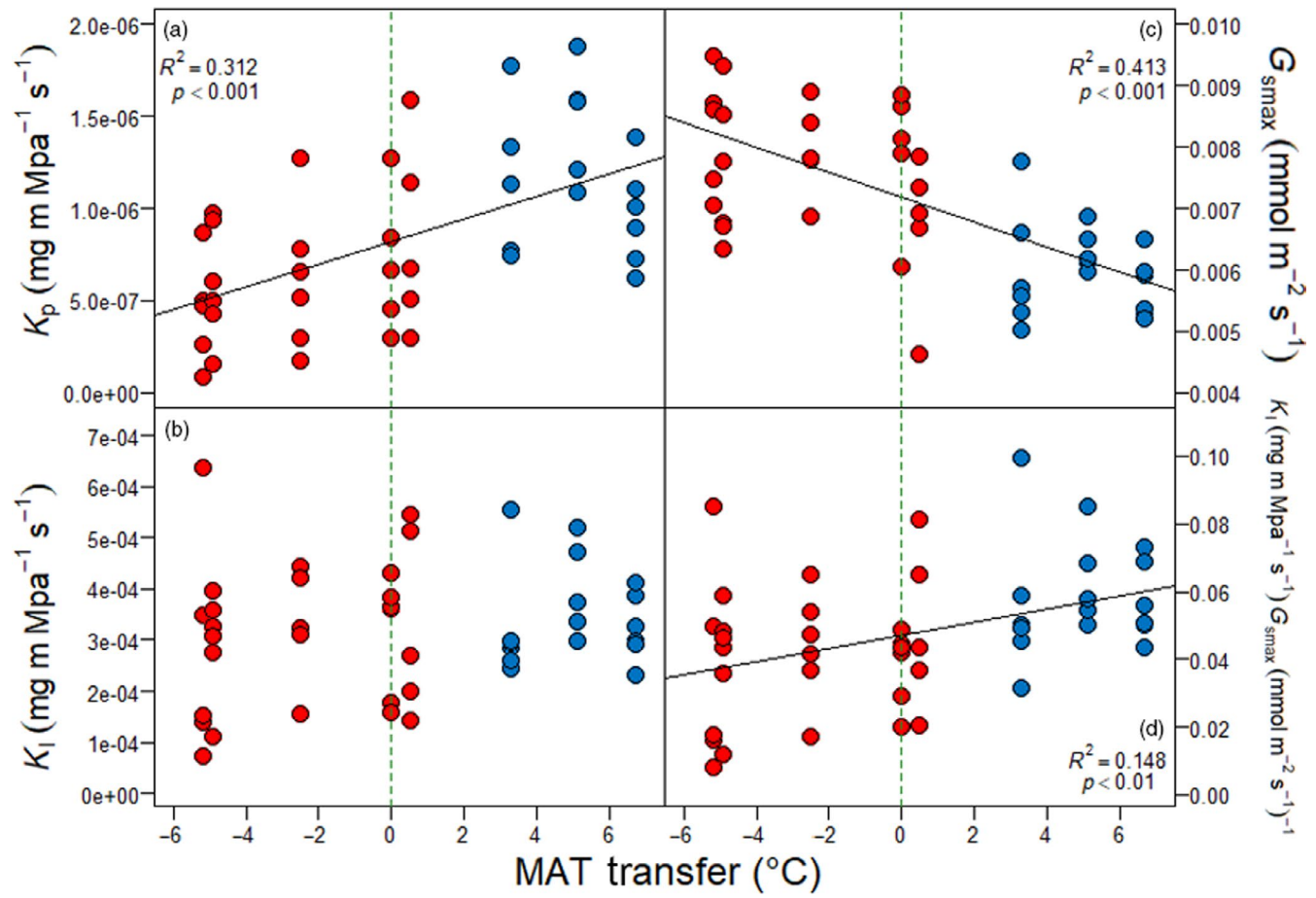


FIGURE 3 Relationship between petiole theoretical hydraulic conductivity (K_p ; mg m⁻¹ MPa⁻¹ s⁻¹), leaf area normalized theoretical hydraulic conductivity of the petiole (K_i ; mg m⁻¹ s⁻¹ MPa⁻¹), leaf theoretical stomatal conductance (G_{smax} ; mmol m⁻² s⁻¹), the ratio between K_i and G_{smax} and source population mean annual temperature MAT transfer in the Sonoran Desert ecotype (red, $n = 30$) and Mogollon Rim ecotype (blue, $n = 18$). Vertical dotted lines indicate the mean annual temperature (MAT °C) of the garden

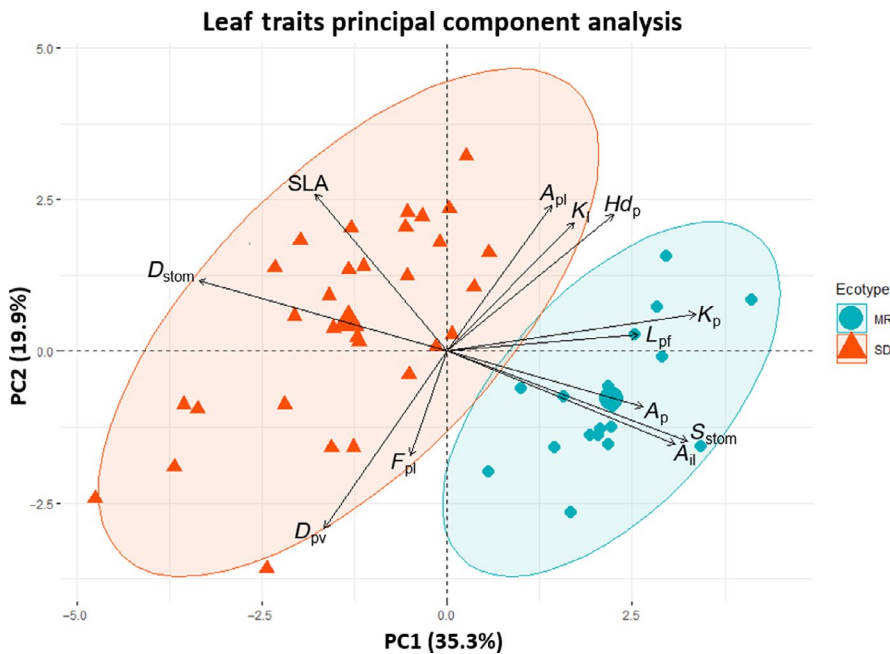


FIGURE 4 Principal component analysis (PCA) summarizing leaf trait spectrum variables at genotype level related with the two ecotypes, Sonoran Desert (SD) and the Mogollon Rim (MR). Plot of PC1 (37.1% of total variation) and PC2 (18.6% variation) showing 95% confidence ellipses of ecotype means

permutation MANOVAs identified similar significant differences at ecotype and population level ($F = 17.97$, $df = 1$, $p > 0.001$; $F = 3.85$, $df = 7$, $p > 0.001$; Figure S1).

3.3 | Whole-plant architecture spectrum

Traits within the architecture spectrum mostly diverged between ecotypes (Table 3). As hypothesized, tree architecture in the MR ecotype enhanced leaf sun exposure while the SD ecotype prioritized transpiration rates of individual leaves. Specifically, A_i and A_c were 20% ($t = -2.26$, $df = 62$, $p < 0.01$, Table 3) and 34% ($t = -4.02$, $df = 46.83$, $p < 0.001$, Table 3) larger in the MR ecotype, respectively while A_s , A_i and H were 38% ($t = 10.9$, $df = 43.5$, $p < 0.001$, Table 3) and 34% larger ($t = 2.34$, $df = 78$, $p < 0.05$, Table 3) in the SD ecotype, respectively (Table 3). However, LAI did not differ between ecotypes due to the higher A_i occurring in more spreading canopies (i.e. higher A_c) of the MR ecotypes. Repeated measures showed that the MR ecotype maintained a larger A_c throughout the growing season ($F = 24.5$, $df = 1$, $p < 0.001$, Table S1), that was independent of the time of year (i.e. the interaction, ecotype \times time was not significant). Similarly, the repeated measures analysis revealed a significant difference between the taller SD and the shorter MR trees ($F = 7.50$, $df = 2$, $p < 0.001$, Table S1), that was also independent of time of year (ecotype \times time was not significant).

We found that PC1 and PC2, explained 35.3% and 25.8% of the variance and were the only significant components in the architecture trait spectrum (Figure 5). However, because PC1 was the only component showing a significant relationship with the *P. fremontii* elevational gradient ($R^2 = 0.57$, $p < 0.001$, Figure S2), we focused our analysis on this axis exclusively. PC1 displayed

simultaneous positive relationships with trait characteristics of the MR ecotype (A_i , A_c and LAI) and negative relationship with the two architectural trait characteristics of the SD ecotype (A_s : A_i and H ; Figure 5). Although the 95% confidence ellipses of both ecotypes overlapped in the biplot (Figure 5), we found a significant difference between the two ecotype PC1 scores ($t = 6.42$, $df = 62$, $p > 0.001$). Interestingly, ANOVA and Tukey's HSD tests detected significant differences between the four highest elevation populations with positive MAT transfer distance, including the only SD population with positive MAT transfer distance, with the four populations having zero or negative MAT transfer distance (Figure S2). Simultaneous analysis of all architecture traits confirmed these significant differences between ecotypes and populations ($F = 14.81$, $df = 1$, $p > 0.001$; $F = 5.54$, $df = 7$, $p > 0.001$; Figure S2).

3.4 | Wood economic spectrum traits

Wood traits related to structural support and frost protection including D_{stem} and F_b were 8% ($t = -4.06$, $df = 46$, $p < 0.001$, Table 3) and 35% ($t = -5.91$, $df = 46$, $p < 0.001$, Table 3) greater in the MR ecotype, respectively. Conversely, in wood traits related to water transport efficiency, we found that Hd_s and F_{sl} were 8% ($t = 2.28$, $df = 46$, $p < 0.05$, Table 3), and 17% ($t = -2.66$, $df = 46$, $p < 0.05$, Table 3) greater in the SD ecotype, respectively. A_{si} and D_{sv} values did not significantly differ between these two ecotypes (Table 3). As expected in an irrigated common garden, we did not find differences in mean Ψ_{pd} throughout the growing season (Table 3). However, we found the SD ecotype displayed more negative mean Ψ_{md} throughout the growing season ($t = -0.56$, $df = 46$, $p < 0.001$, Table 3). Repeated measures detected significant Ψ_{pd}

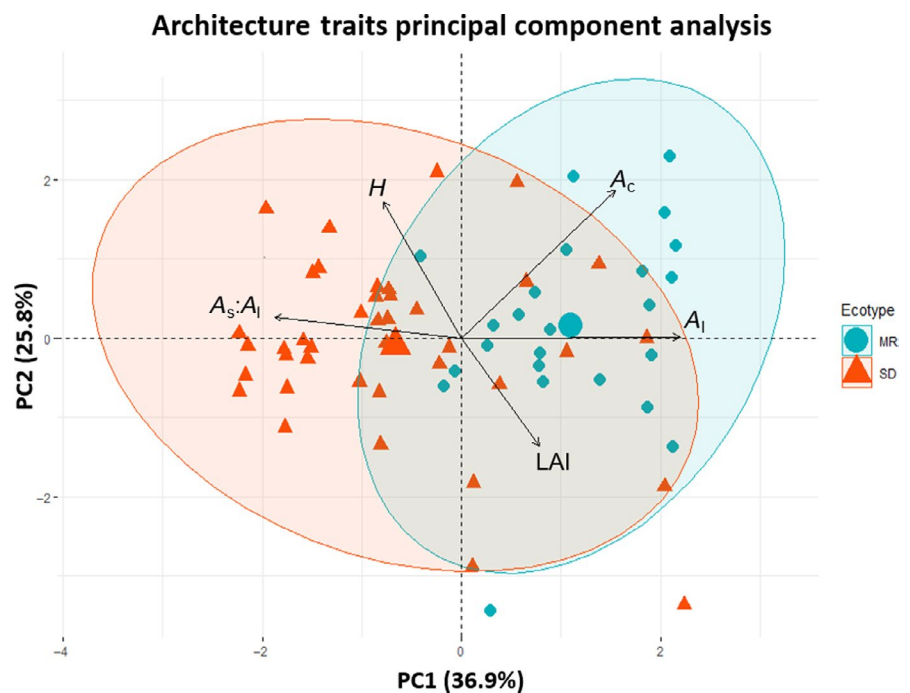


FIGURE 5 Principal component analysis (PCA) summarizing the whole-plant architecture traits spectrum variables at genotype level related with the two ecotypes, Sonoran Desert (SD) and the Mogollon Rim (MR). Plot of PC1 (45.2% of total variation) and PC2 (30.8% variation) showing 95% confidence ellipses of ecotype means

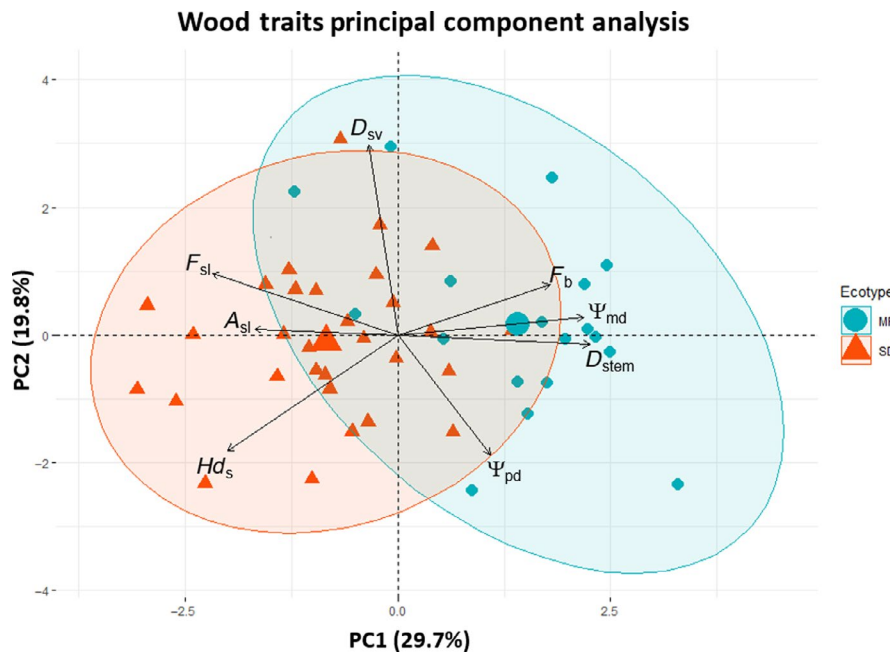


FIGURE 6 Principal component analysis (PCA) summarizing wood traits spectrum variables at genotype level related with the two ecotypes, Sonoran Desert (SD) and the Mogollon Rim (MR). Plot of PC1 (29.7% of total variation) and PC2 (19.8% variation) showing 95% confidence ellipses of ecotype means

differences among the five measurement periods ($F = 15.8$, $df = 1$, $p < 0.001$, Table S1), but no differences were detected in Ψ_{pd} between ecotypes or the interaction ecotype \times time (Table S1). On the other hand, Ψ_{md} exhibited significant differences between ecotypes ($F = 23.6$, $df = 1$, $p < 0.001$, Table S1) and time ($F = 112.7$, $df = 4$, $p < 0.001$, Table S1) while the interaction ecotype \times time was not significant.

In the wood spectrum PCA, three principal components which together explained 64% of the variation were significant. However, only PC1, accounting for 29.7% of the variation, was correlated with MAT transfer distance ($R^2 = 0.37$, $p < 0.001$; Figure S3). PC1 also exhibited significant positive correlations with D_{stem} , Ψ_{md} and F_b while showing negative correlations with F_{sl} , H_{d_s} and A_{sl} (Figure 6). Like the architecture trait PCA, the 95% confidence ellipses of both ecotypes overlapped but contrasts between ellipses were still detected ($t = 6.86$, $df = 46$, $p < 0.001$). Nevertheless, ANOVA and Tukey's HSD tests only detected differences between the lowest elevation population with the most negative MAT transfer distance (-5.2°C) and the three populations with the most positive MAT transfer distance (Figure S3). PERMANOVA and pairwise permutation MANOVAs tests revealed significant differences between ecotypes ($F = 9.31$, $df = 1$, $p > 0.001$; Figure S3) and among populations ($F = 2.42$, $df = 7$, $p > 0.001$; Figure S3).

3.5 | PCA analysis of pooled traits

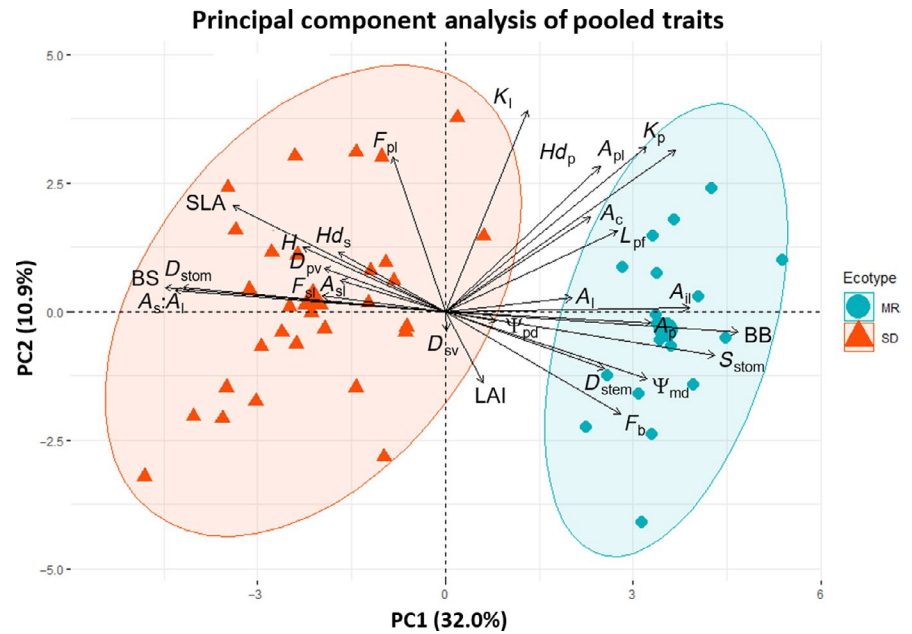
A PCA of all 27 traits measured required eight components with eigenvalues greater than 1 to reach 78% of total variance. However, PC1 was the only axis of the PCA that was significant accounting for 32% of the total variance. Likewise, PC1 yielded a significant correlation with MAT transfer distance of source populations ($R^2 = 0.84$, $p < 0.001$; Figure S4). Additionally, we found PC1 displaying

significant negative correlations with traits characteristic of the SD ecotype while observing the opposite trend with traits associated with the MR ecotype (Figure 7). Therefore, the SD ecotype 95% confidence ellipse was found in the negative half of PC1 axis enclosing the vectors representing BS, $A_s:A_l$, D_{stom} , SLA, H , F_{sl} , D_{pv} , A_{sl} and H_{d_s} . In the positive half of the biplot, we observed the MR ellipse enclosing the BB, S_{stom} , A_{il} , K_p , Ψ_{md} and F_b , L_{pf} , D_{stem} , H_{d_p} , A_c and A_l vectors (Figure 7). Differences between the ecotypes along the PC1 axis were highly significant ($t = -17.03$, $df = 46$, $p < 0.001$), and a PERMANOVA test confirmed these differences ($F = 17.84$, $df = 1$, $p > 0.001$).

Although the relationships between the two ecotypes and the 27 different traits elucidate important features regarding climate adaptation at the regional scale, trait differentiation at the population-level can increase our understanding of adaptation at the local level. We found that the SD population with the largest mean warmest monthly temperature (MWMT), elevation 161 m (Table S3), displayed A_{il} , SLA, S_{stom} , L_{pf} , A_l , $A_s:A_l$, A_c , H , K_p and D_{stem} with the most extreme values within the ecotype (Tables S2, S3, S4 and S5). Similar results were obtained in the MR ecotype. Specifically, the population with the lowest mean coldest monthly temperature (MCMT), elevation 1940 (Table 3), exhibited the most extreme A_{il} , SLA, D_{stem} , A_l , A_c and Ψ_{md} within the ecotype (Tables S3, S5 and S6). Additionally, we found significant positive relationships between elevation and A_{il} , S_{stom} , A_p , L_{pf} , A_l , A_c , D_{stem} and F_b (Tables S2, S3, S4 and S5). Likewise, source population elevation had a negative relationship with D_{stom} , G_{smax} , SLA, K_p , H , $A_s:A_l$, A_{sl} and Ψ_{md} (Tables S2, S3, S4 and S5).

To gain a better understanding of trait variability in each ecotype, we constructed 95% confidence ellipses for the eight populations that made up the two ecotypes in the same PCA of all 27 traits (Figure 8). As expected, we found low elevation—negative MAT transfer distance—populations ellipses (SD ecotype) were mainly placed in the negative

FIGURE 7 Principal component analysis (PCA) summarizing all 27 traits variables at genotype level related with the two ecotypes, Arizona Sonoran Desert (SD) and the Mogollon Rim (MR). Plot of PC1 (32% of total variation) and PC2 (10.9% variation) showing 95% confidence ellipses of ecotype means



Principal component analysis of pooled traits by population

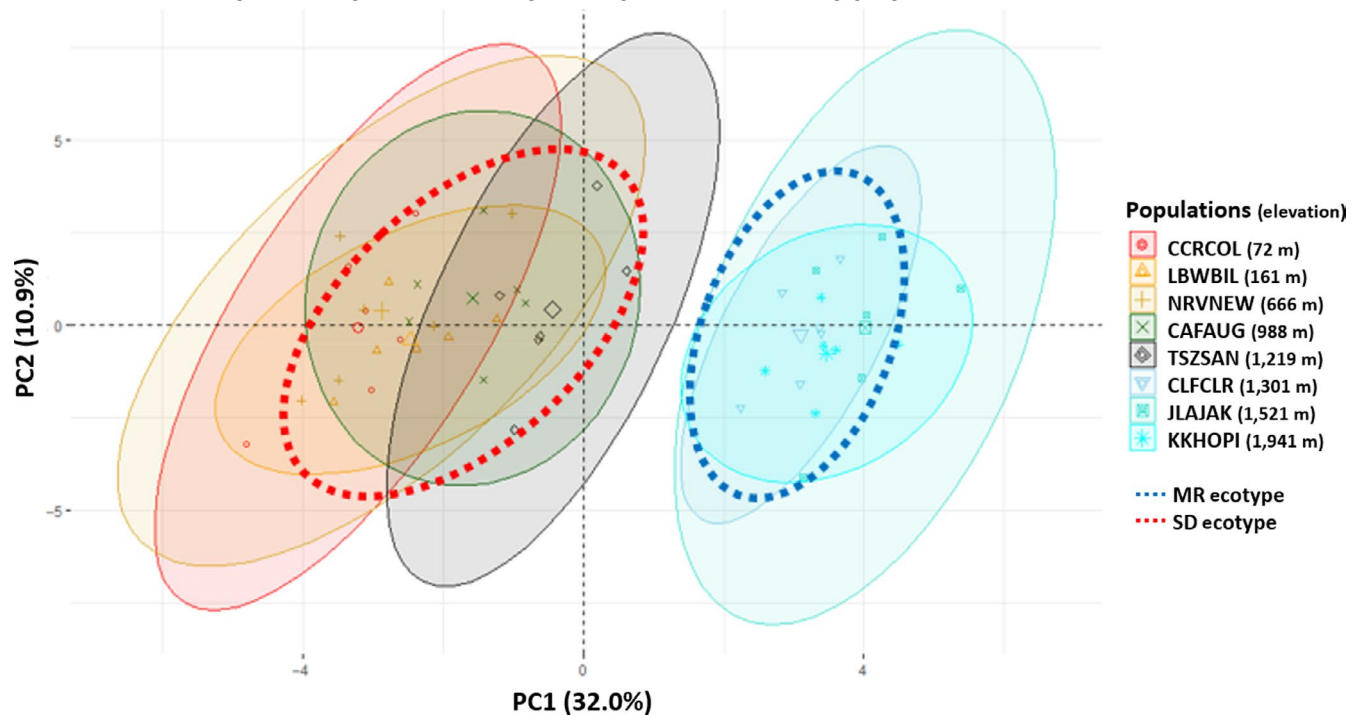


FIGURE 8 Principal component analysis (PCA) summarizing all 27 traits variables at genotype level related with eight populations that collectively represent the entire elevational range of the species. Plot of PC1 (32% of total variation) and PC2 (10.9% variation) showing 95% confidence ellipses of population means

half of the PC1 axis while the three high elevation populations (MR ecotype) remained in the right half of PC1 (Figure 8). However, as suggested by the larger size SD ecotype ellipses in the leaf, architecture and all 27 traits PCA biplots, we observed larger variability in the locations occupied by the five SD populations' ellipses. Particularly, we found that the San Pedro Riparian National Conservation Area

(TSZSAN) population in southern Arizona (1,212 m) and to a lesser extent the Agua Fria National Monument (CAFAUG) population (988 m) in central Arizona displayed ellipses expanded towards the positive, MR characteristic, area of the PC1 axis. Although these populations mainly displayed trait characteristics of the SD ecotype, it is evident that they have some morpho-physiological trait characteristics found

in the MR ecotype. Based exclusively on the PC1 scores using an ANOVA and Tukey's HSD test, we found significant differences between the five SD and the three MR ecotype populations (Figure S4). Therefore, the TSZSAN and CAFAUG populations did not differ from the other 3 SD ecotype populations. However, using a PERMANOVA and pairwise permutation MANOVAs on all 27 traits simultaneously, we found the significant population differences ($F = 4.07$, $df = 7$, $p > 0.001$; Figure S4). Specifically, the TSZSAN population significantly differed from all other SD ecotype populations except for the CAFAUG population. Simultaneously, the CAFAUG population only significantly differed from all MR populations and the lowest elevation population of the SD ecotype.

3.6 | RDA analysis of pooled traits with environmental predictors

RDA and PCA ordination techniques of all 27 traits showed general similar trait patterns in their respective biplot and triplot (Figures 7

and 9). Forward selection of environmental predictors (provenance latitude, longitude, mean annual precipitation, MAT transfer distance) revealed that MAT transfer distance, MAP (mean annual precipitation) and elevation were the only three variables that significantly explain trait variation in *P. fremontii*. However, elevation had to be dropped from the analysis because it displays high collinearity with MAT transfer distance. Ecotype grouping which also showed to explain trait variation was included in the analysis as a categorical genetic predictor.

RDA Axis 1 described 30.6% of the variation in all 27 traits (compared to 32.3% in the PCA). This axis displayed highly significant relationships with MAT transfer distance and both ecotypes. RDA analysis found that the amount of variance explained by these predictor variables (i.e. constrained variances) was 32% while the unconstrained variance (i.e. the amount of variance remaining in the response variables) was 68%. Although Axis 2 described only 2.4% of the variation (compared to 10.9% in the PCA) and was not significant, it was correlated with MAP (environmental predictor), hydraulic efficiency traits (D_{pv} , F_{sl} , F_{pl}), whole canopy traits (LAI, A_l , A_s , A_l , H) and wood trait D_{stem} (Figure 9).

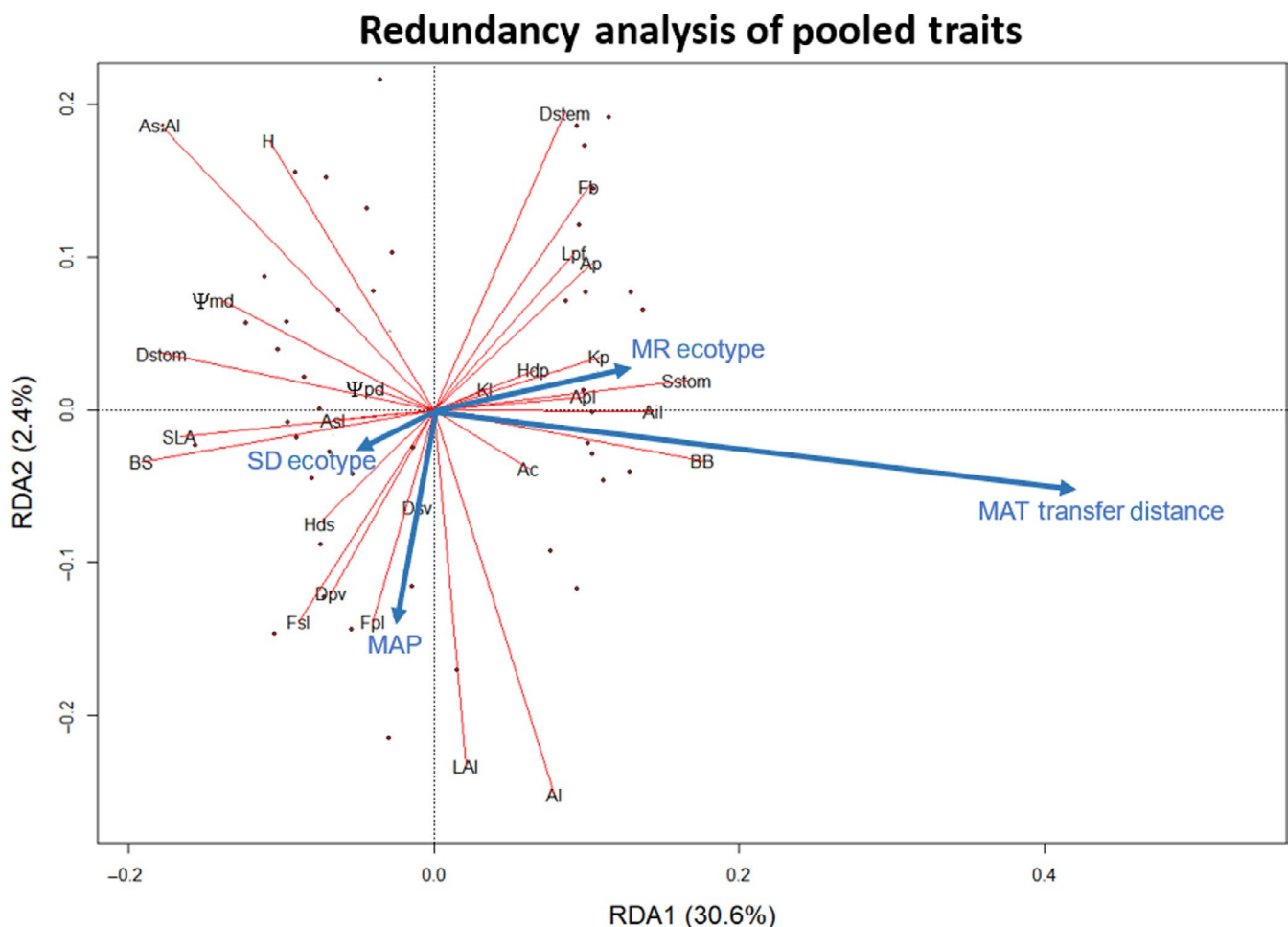


FIGURE 9 Redundancy analysis triplot with explanatory variables (Transfer.MAT = transfer mean annual temperature, MAP = population mean annual precipitation and the two ecotypes) and all 27 traits as response variables. Individual genotypes ($n = 48$) are marked as red dots. The relationship between the explanatory variables (blue vectors) and response variables (red vectors) can be interpreted by the alignment of the vectors

4 | DISCUSSION

Our results demonstrated that local adaptation of *P. fremontii* populations over its geographical distribution comprises many different traits that are coordinated across multiple scales from epidermal and vascular tissue to individual organ and whole-plant architecture. These findings support our economic spectrum similarity hypothesis, and more broadly adaptive syndrome theory, postulating that many traits are expressed within an ecotype to best survive their specific environment (Rueda et al., 2018). The coordination of traits indicates that *P. fremontii* is comprised of genotypes that are highly specialized to cope with local environmental conditions and have resulted in the evolution of ecotypes at regional levels that each have a suite of adaptive traits (an adaptive syndrome) that make each best adapted to its ecoregion. Simultaneously, we found finer differences in trait coordination at the population level that reflect gradual adaptation strategies at local environmental conditions. Thus, results underscore the potential importance of using assisted migration as a possible solution to restoration of *Populus* species conducted under rapidly shifting climate conditions.

4.1 | Adaptive syndrome trait correlations within the MR ecotype

Late budburst and early budset of the high latitude/elevation MR ecotype revealed an adaptive trade-off between avoiding freezing temperatures and maximizing growth (Cooper et al., 2019; Evans et al., 2016; Fischer et al., 2017; Friedman et al., 2011; Grady et al., 2015). Our results paralleled previous research using all 16 populations in the same mid-elevation common garden as the one used in the present study (Cooper et al., 2019). However, Cooper et al. (2019) also repeatedly measured phenology in two additional replicated gardens that represent the two extreme edges of *P. fremontii*'s climatic distribution to estimate phenological plasticity. Interestingly, the warm-adapted SD ecotype trees displayed greater phenological plasticity than the cold-adapted MR ecotype trees, reflecting the extent to which exposure to freezing temperatures acts as an agent of selection in cold-adapted genotypes (Cooper et al., 2019; Hultine, Froend, et al., 2020). On the other hand, phenological characteristics, i.e. earlier budburst, later budset) displayed by SD ecotype trees may have resulted from the combined effects of infrequent exposure to freezing temperatures, longer optimal growing seasons and extreme mid-summer temperatures in the Sonoran Desert that limits net carbon gain.

Previous investigations have found that plants with thicker stems and larger leaves are frequently accompanied by less frequent branching with wider branching angles (Cornelissen, 1999; Corner, 1949; Trueba et al., 2016; Wright & Westoby, 2002). Accordingly, we found larger leaves and canopies areas to be characteristic traits of the MR ecotype (Table 3). The larger A_c in the MR ecotype trees may reflect selection to maximize sun exposure and limit self-shading. Additionally, the MR trees had leaves with petioles that were more elliptical (i.e. flattened) compared to the SD ecotype. Past investigations on *P. fremontii*

have identified the flattened non-rigid petioles oriented perpendicular to the blade to be responsible for the characteristic fluttering of leaves under breezy conditions (Niklas, 1991; Roden & Pearcy, 1993). Other previous studies have concluded that leaf fluttering maximizes carbon gain homogenizing light distribution throughout the multi-layered canopy (Sprugel, 1989). Thus, in trees with larger A_{ij} , A_c , A_l and shorter growing season lengths, the characteristic petiole flattened-leaf flutter combined with broader branching canopies might increase the number of leaves operating in near optimal light-quenching conditions by reducing leaf shading throughout the day. The genetic basis of these architectural traits is also consistent with other cottonwood studies showing that the fractal architecture of different tree genotypes is genetically based and heritable (Bailey et al., 2004), which affects sink-source relationships and herbivores such as aphids (Compson et al., 2011).

In accordance with our hypothesis, MR ecotype trees exhibited a suite of conservative hydraulic traits that together represent an adaptive syndrome resulting in higher survival to freezing temperatures (Chave et al., 2009; Körner, 2003; Sperry & Sullivan, 1992). Susceptibility to freeze-thaw-induced xylem cavitation increases with vessel size because air bubbles are more easily released from the dissolution of gas during thawing in larger diameter vessels (Mayr & Sperry, 2010; Sperry & Sullivan, 1992). Consequently, the Hd_s was significantly lower in MR stems, reflecting the presence of smaller diameter vessels relative to SD stems. Similarly, Hd_s has been correlated with sapwood area-specific hydraulic conductivity (Hajek et al., 2014; Kolb & Sperry, 1999). The reduced hydraulic efficiency in many of the wood xylem traits may explain why compared with SD trees, the MR ecotype leaves displayed lower mean D_{stom} and G_{smax} values, reflecting an upper bound on water delivery from woody tissues to the canopy.

On the other hand, the MR trees displayed higher values for traits that are characteristic for high tissue structural integrity and frost protection, including D_{stem} and F_b . Although D_{stem} is correlated with a reduced hydraulic conductivity (Reich, 2014), it has been correlated with greater mechanical support against xylem implosion by negative pressure (cavitation resistance) caused by low xylem water potentials (Hacke et al., 2001) and wood mechanical strength (Chave et al., 2009; Niklas & Spatz, 2010, 2012). Bark in broadleaved species has been found to be a better thermal insulator than conifer bark (Pásztor & Ronyecz, 2013) while stem shrinkage associated with freeze-thaw cycles has been correlated with the thickness of the bark (Améglio et al., 2001; Zweifel & Häsler, 2000). Consequently, in angiosperms around the world, outer bark thickness has been found to increase in environments with temperature seasonality (Rosell, 2016). Bark thickness has also been associated with the protection of phloem and other living tissues from freezing temperatures (Améglio et al., 2001; Arco Molina et al., 2016; Charrier et al., 2017).

4.2 | Adaptive syndrome trait correlations within the SD ecotype

As we hypothesized, the SD ecotype featured a coordinated suite of functional traits (i.e. a different adaptive syndrome) that prioritize

greater water transport efficiency to reduce foliar thermal load via enhanced evaporative cooling. Thus, the SD ecotype displayed smaller leaves with a potentially reduced exposure to short-wave radiation from sunlight. Likewise, the thinner leaves with higher SLA likely have a lower thermal capacitance—or heat storage over time—than similar sized leaves with a lower SLA. Additionally, SD ecotype leaves displayed a relatively high D_{stom} and low S_{stom} arrangement, which allows the leaf to rapidly adjust stomatal conductance to changes in air temperatures and humidity (Hetherington & Woodward, 2003).

Because leaves with smaller S_{stom} display smaller cross-sectional area of the guard cells and reduced pore depths, these leaves can achieve a greater stomatal conductance (g_s) per unit area occupied by stomata (Franks & Farquhar, 2007). Accordingly, we found that based on their stomatal morphological characteristics, SD trees exhibited a larger theoretical G_{smax} than the MR ecotype. Many Sonoran Desert ecotype trees are exposed to mid-summer temperatures that approach or even exceed 50°C. These extreme temperatures can simultaneously damage the electron transport capacity of Photosystem II and increase photorespiration (Allakhverdiev et al., 2008; Hultine, Froend, et al., 2020; O'Sullivan et al., 2017). Therefore, warm-adapted trees likely prioritize maintaining midday leaf conductance to evaporatively cool the canopy (Fauset et al., 2018; Hultine, Allan, et al., 2020; Hultine, Froend, et al., 2020; Michaletz et al., 2015). The combination of these leaf morpho-physiological features allows SD trees to achieve higher levels of transpirational cooling of their leaves while reducing heat gain from incident light radiation (Hultine, Allan, et al., 2020; Hultine, Froend, et al., 2020). For example, another recent study using genotypes from the same common garden as the present study reported that the SD ecotype trees displayed 35% higher midday leaf transpiration rates and 4°C lower leaf temperature than the MR ecotype trees (Hultine, Allan, et al., 2020).

Repeated measures of A_{li} and SLA indicated SD trees continuously displayed smaller and thinner leaves as an additional possible adaptation to summer extreme temperatures during the growing season (Table S1). The reduced leaf size, relative to the MR leaves, suggest that the SD trees displayed more rapid turnover rates of leaves with cheaper construction costs over the growing season. This might be due to the high cost of maintaining leaves relative to their return in carbon during the hottest part of the summer. Extreme high temperatures negatively affect the carbon balance of leaves by simultaneously reducing photosynthesis and increasing respiration (Haworth et al., 2018; Sharkey, 2005).

Greater investment in the construction of larger leaves and larger petioles in MR leaves was associated with having a greater theoretical K_p . However, the higher K_p was offset by the larger leaf area and thus K_l was uniform across the two ecotypes. Additionally, we found a significant positive relationship between positive MAT transfer distance or elevation and the ratio between K_l (supply) and G_{smax} (demand) at the population level. These results imply that SD ecotype trees possess a set of leaf morphological traits that allow larger and faster utilization of water for transpiration, but at the risk of greater leaf water demand relative to supply via the petiole. Measurements

of leaf Ψ_{md} appeared to reflect a greater hydraulic risk strategy and weaker stomatal control over plant water potential in SD ecotype trees (Table S1). Specifically, mean Ψ_{md} measured over the growing season regularly fell below −1.88 MPa; the xylem pressure at which hydraulic failure has been previously reported to occur in *P. fremontii* (Choat et al., 2012; Joshua Leffler et al., 2000; Li et al., 2008; Table S1). Given these results, it appears that SD ecotype trees take on a risky trade-off strategy between maximizing delivery to the canopy at the expense of increasing vulnerability to cavitation which may limit these trees to river reaches with predictable and abundant groundwater availability during the entire growing season.

Alternatively, the risky water use strategy in SD trees may have been partially mitigated by maintaining a substantially higher $A_s:A_l$ relative to the MR ecotype trees. Given that SD trees have most likely been selected to maximize canopy thermal regulation via evaporative cooling, it was not surprising that at the whole tree level, water supply (i.e. A_s) relative to demand (i.e. A_l) was high relative to MR trees. Seasonal increases in $A_s:A_l$ has been reported to be a strategy in other species to increase water supply to canopies during summer drought or under high temperature (Carter & White, 2009; Eamus et al., 2000; O'Grady et al., 2009). Similarly, a previous investigation in *P. fremontii* observed that $A_s:A_l$ was correlated with groundwater availability (Gazal et al., 2006). Accordingly, SD trees exhibited higher $A_s:A_l$ coupled with a greater F_{si} and Hd_s that reflects the greater hydraulic efficiency to meet the higher water demand for leaf evaporative cooling (Drake et al., 2018; Gleason et al., 2012; Sterck et al., 2008; Zaehle, 2005).

4.3 | Trait contrasts among populations

Differences in functional traits in *P. fremontii* at the population level resembled differences between the two ecotypes. However, we detected finer variations in phenotypic characteristics across the climatic gradient in which the eight populations were sourced from. This was particularly true among the SD ecotype populations. Specifically, middle elevation TSZSAN population which displayed slight intermediate trait characteristics between the two ecotypes. Due to the geographical and environmental characteristics of its source site (southernmost latitude and middle range climate), this population seems to display trait characteristic that reflect climatic adaptation to its intermediate local environmental conditions.

Thus, while displaying SD ecotype characteristics in most LES and WES spectra traits, TSZSAN population exhibited intermediate D_{stom} , A_l and H between the two ecotypes (Tables S2, S4 and S5). Additionally, $A_s:A_l$ in this population was more characteristic of the MR ecotype even though it is the southernmost geographically located of population of the SD ecotype. Consequently, multivariate analyses clustered this population with the MR ecotype populations in the architecture trait spectrum and as its own intermediate group in the WES and the pooled all traits PCA (Figures S2, S3 and S4). Although the 95% confidence intervals representing the TSZSAN populations overlapped the other four SD ecotype populations, its

horizontal range (PC1) exhibited a clear tendency towards the positive, MR ecotype side of the PC1 (Figure 8).

4.4 | Climate change implications

Drought – inter-drought cycles and extreme temperature swings will likely become amplified throughout most of the planet over the next several decades as a consequence of climate change (Garfin et al., 2013; Williams et al., 2020). Results from the present study underscore how extreme events will likely lead to widespread maladaptation and reduced fitness in *Populus* species in response to climate change. For example, the SD ecotype displayed greater capacity to supply water to their canopies to avoid thermal stress but potentially at the expense of being more susceptible to hydraulic dysfunction caused by maintaining lower minimum water potentials, having a higher theoretical maximum stomatal conductance, and having a larger mean hydraulic diameter in woody stems. Thus, increases in drought frequency can be expected to reduce the habitat niche of SD genotypes to locations where soil water availability remains stable independent of drought, such as along the margins of perennially flowing streams (Hultine, Allan, et al., 2020). The MR ecotype, on the other hand, displayed a set of morphological traits designed to increase sunlight exposure and maximize safety from freeze-thaw cavitation, but as a consequence may be unable to cool their canopies when exposed to episodic heatwaves that are likely to increase in frequency and intensity. What remains an open question is whether trait expression is plastic enough to overcome rapid changes in environmental conditions. As the size of the SD ecotype ellipses of the leaf, architecture and pooled traits PCAs showed, the SD ecotype exhibited greater trait variability, perhaps a reflection of greater trait plasticity or higher genetic diversity among genotypes relative to the MR ecotype.

The combination of multiple functional trait spectra demonstrates adaptive syndromes for different ecoregions and present a powerful way to enhance our mechanistic understanding of local adaptation within species. As regional mean annual temperature, drought severity and heat wave occurrence increase over the next several decades, this research improves our understanding of the possible effect that these changes will have on *P. fremontii* and other widely distributed *Populus* species across their geographical ranges. Results therefore, improve our capacity to match genotypes with traits that may yield greater resistance to changing environmental conditions of a given location, and therefore the detection of genotypes best suited for possible repopulation efforts along a species' historical geographical distribution.

ACKNOWLEDGEMENTS

This research was supported by a Huizingh Desert Research Fellowship awarded to DEB, and by the National Science Foundation MacroSystems Biology program [DEB-1340852 (G.J.A.) and DEB-1340856 (K.R.H.)], and MRI-DBI-1126840 (S.A.C., T.G.W.). We thank Arizona Game and Fish in the Agua

Fria national Monument Horseshoe ranch. We would like to thank Christopher Updike, Zachary Ventrella along with several volunteers for help establishing and maintaining the Agua Fria common garden. We also thank Dr Donna Dehn for assistance developing laboratory protocols, Hazel Overturf, Janet Gordon and Premel Patel for assistance in data visualization, Bethany Zumwalde for assistance in the laboratory and in the field.

AUTHORS' CONTRIBUTIONS

D.E.B. and K.R.H. designed the research; D.E.B. and D.F.K. collected the data and performed the analysis; K.C.G., G.J.A., C.A.G., S.A.C., T.G.W. and K.R.H. all contributed the funding to establish, design and maintain the common garden, and all authors contributed to the writing of the manuscript.

PEER REVIEW

The peer review history for this article is available at <https://publons.com/publon/10.1111/1365-2745.13557>.

DATA AVAILABILITY STATEMENT

Data available from the Dryad Digital Repository <https://doi.org/10.5061/dryad.gf1vhhmn9> (Blasini et al., 2020).

ORCID

Davis E. Blasini  <https://orcid.org/0000-0001-5005-9009>

Gerard J. Allan  <https://orcid.org/0000-0002-8007-4784>

Kevin R. Hultine  <https://orcid.org/0000-0001-9747-6037>

REFERENCES

- Ackerly, D., Knight, C., Weiss, S., Barton, K., & Starmer, K. (2002). Leaf size, specific leaf area and microhabitat distribution of chaparral woody plants: Contrasting patterns in specieslevel and community level analyses. *Oecologia*, 130(3), 449–457. <https://doi.org/10.1007/s004420100805>
- Allakhverdiev, S. I., Kreslavski, V. D., Klimov, V. V., Los, D. A., Carpentier, R., & Mohanty, P. (2008). Heat stress: An overview of molecular responses in photosynthesis. *Photosynthesis Research*, 98(1–3), 541–550. <https://doi.org/10.1007/s11120-008-9331-0>
- Améglio, T., Cochard, H., & Ewers, F. W. (2001). Stem diameter variations and cold hardiness in walnut trees. *Journal of Experimental Botany*, 52(364), 2135–2142. <https://doi.org/10.1093/jexbot/52.364.2135>
- Anderson, M. J. (2001). A new method for non-parametric multivariate analysis of variance. *Austral Ecology*, 26(1), 32–46. <https://doi.org/10.1046/j.1442-9993.2001.01070.x>
- Ansley, R. J., Mirik, M., Surber, B. W., & Park, S. C. (2012). Canopy area and aboveground mass of individual redberry juniper (*Juniperus pinchotii*) trees. *Rangeland Ecology and Management*, 65(2), 189–195. <https://doi.org/10.2111/REM-D-11-00112.1>
- Arco Molina, J. G., Hadad, M. A., Patón Domínguez, D., & Roig, F. A. (2016). Tree age and bark thickness as traits linked to frost ring probability on *Araucaria araucana* trees in northern Patagonia. *Dendrochronologia*, 37, 116–125. <https://doi.org/10.1016/j.dendro.2016.01.003>
- Bailey, J. K., Bangert, R. K., Schweitzer, J. A., Trotter, R. T., Shuster, S. M., & Whitham, T. G. (2004). Fractal geometry is heritable in trees. *Evolution*, 58(9), 2100–2102. <https://doi.org/10.1111/j.0014-3820.2004.tb00493.x>
- Barbour, M. A., Rodriguez-Cabal, M. A., Wu, E. T., Julkunen-Tiitto, R., Ritland, C. E., Miscampbell, A. E., Jules, E. S., & Crutsinger, G. M. (2015).

- Multiple plant traits shape the genetic basis of herbivore community assembly. *Functional Ecology*, 29(8), 995–1006. <https://doi.org/10.1111/1365-2435.12409>
- Bates, D., Mächler, M., Bolker, B., & Walker, S. (2015). Fitting linear mixed-effects models using lme4. *Journal of Statistical Software*, 67(1). <https://doi.org/10.18637/jss.v067.i011>
- Blasini, D. E., Koepke, D. F., Grady, K. C., Allan, G. J., Gehring, C. A., Whitham, T. G., Cushman, S. A., & Hultine, K. R. (2020). Data from: Adaptive trait syndromes along multiple economic spectra define cold and warm adapted ecotypes in a widely distributed foundation tree species. *Dryad Digital Repository*, <https://doi.org/10.5061/dryad.gf1vhhm9>
- Borcard, D., Gillet, F., & Legendre, P. (2011). *Numerical ecology with R*. Springer. <https://doi.org/10.1007/978-1-4419-7976-6>
- Buesa, R. J., & Peshkov, M. V. (2009). Histology without xylene. *Annals of Diagnostic Pathology*, 13(4), 246–256. <https://doi.org/10.1016/j.anndiagpath.2008.12.005>
- Carter, J. L., & White, D. A. (2009). Plasticity in the Huber value contributes to homeostasis in leaf water relations of a mallee Eucalypt with variation to groundwater depth. *Tree Physiology*, 29(11), 1407–1418. <https://doi.org/10.1093/treephys/tpq076>
- Chapin, F. S., Matson, P. A., & Vitousek, P. M. (2011). *Principles of terrestrial ecosystem ecology*. Springer. <https://doi.org/10.1007/978-1-4419-9504-9>
- Charrier, G., Nolf, M., Leitinger, G., Charra-Vaskou, K., Losso, A., Tappeiner, U., Améglio, T., & Mayr, S. (2017). Monitoring of freezing dynamics in trees: A simple phase shift causes complexity. *Plant Physiology*, 173(4), 2196–2207. <https://doi.org/10.1104/pp.16.01815>
- Chave, J., Coomes, D., Jansen, S., Lewis, S. L., Swenson, N. G., & Zanne, A. E. (2009). Towards a worldwide wood economics spectrum. *Ecology Letters*, 12(4), 351–366. <https://doi.org/10.1111/j.1461-0248.2009.01285.x>
- Choat, B., Jansen, S., Brodribb, T. J., Cochard, H., Delzon, S., Bhaskar, R., Bucci, S. J., Feild, T. S., Gleason, S. M., Hacke, U. G., Jacobsen, A. L., Lens, F., Maherali, H., Martínez-Vilalta, J., Mayr, S., Mencuccini, M., Mitchell, P. J., Nardini, A., Pittermann, J., ... Zanne, A. E. (2012). Global convergence in the vulnerability of forests to drought. *Nature*, 491(7426), 752–755. <https://doi.org/10.1038/nature11688>
- Clausen, J., Keck, D. D., & Hiesey, W. M. (1940). Experimental studies on the nature of species. I. Effect of varied environments on western North American plants. *Carnegie Institution of Washington Publication*. <https://doi.org/10.1086/280930>
- Cochard, H., Forestier, S., & Améglio, T. (2001). A new validation of the Scholander pressure chamber technique based on stem diameter variations. *Journal of Experimental Botany*, 52(359), 1361–1365. <https://doi.org/10.1093/jexbot/52.359.1361>
- Compson, Z. G., Larson, K. C., Zinkgraf, M. S., & Whitham, T. G. (2011). A genetic basis for the manipulation of sink–source relationships by the galling aphid *Pemphigus batae*. *Oecologia*, 167(3), 711–721. <https://doi.org/10.1007/s00442-011-2033-x>
- Cooper, H. F., Grady, K. C., Cowan, J. A., Best, R. J., Allan, G. J., & Whitham, T. G. (2019). Genotypic variation in phenological plasticity: Reciprocal common gardens reveal adaptive responses to warmer springs but not to fall frost. *Global Change Biology*, 25(1), 187–200. <https://doi.org/10.1111/gcb.14494>
- Cornelissen, J. H. C. (1999). A triangular relationship between leaf size and seed size among woody species: Allometry, ontogeny, ecology and taxonomy. *Oecologia*, 118(2), 248–255. <https://doi.org/10.1007/s004420050725>
- Cornelissen, J. H. C., Lavorel, S., Garnier, E., Díaz, S., Buchmann, N., Gurvich, D. E., Reich, P. B., Steege, H. T., Morgan, H. D., Heijden, M. G. A. V. D., Pausas, J. G., & Poorter, H. (2003). Handbook of protocols for standardised and easy measurement of plant functional traits worldwide. *Australian Journal of Botany*, 51(4), 335–380. <https://doi.org/10.1071/BT02124>
- Corner, E. J. H. (1949). The Durian theory or the origin of the modern tree. *Annals of Botany*, 13(4), 367–414. <https://doi.org/10.1093/oxfordjournals.aob.a083225>
- Cushman, S. A., Max, T., Meneses, N., Evans, L. M., Ferrier, S., Honchak, B., Whitham, T. G., & Allan, G. J. (2014). Landscape genetic connectivity in a riparian foundation tree is jointly driven by climatic gradients and river networks. *Ecological Applications*, 24, 1000–1014.
- de Villemereuil, P., Schielzeth, H., Nakagawa, S., & Morrissey, M. (2016). General methods for evolutionary quantitative genetic inference from generalized mixed models. *Genetics*, 204(3), 1281–1294. <https://doi.org/10.1534/genetics.115.186536>
- Denny, E. G., Gerst, K. L., Miller-Rushing, A. J., Tierney, G. L., Crimmins, T. M., Enquist, C. A. F., Guertin, P., Rosemartin, A. H., Schwartz, M. D., Thomas, K. A., & Weltzin, J. F. (2014). Standardized phenology monitoring methods to track plant and animal activity for science and resource management applications. *International Journal of Biometeorology*, 58(4), 591–601. <https://doi.org/10.1007/s00484-014-0789-5>
- Drake, J. E., Tjoelker, M. G., Vårhammar, A., Medlyn, B. E., Reich, P. B., Leigh, A., Pfautsch, S., Blackman, C. J., López, R., Aspinwall, M. J., Crous, K. Y., Duursma, R. A., Kumarathunge, D., De Kauwe, M. G., Jiang, M., Nicotra, A. B., Tissue, D. T., Choat, B., Atkin, O. K., & Barton, C. V. M. (2018). Trees tolerate an extreme heatwave via sustained transpirational cooling and increased leaf thermal tolerance. *Global Change Biology*, 24(6), 2390–2402. <https://doi.org/10.1111/gcb.14037>
- Eamus, D., O'Grady, A. P., & Hutley, L. (2000). Dry season conditions determine wet season water use in the wet-tropical savannas of northern Australia. *Tree Physiology*, 20(18), 1219–1226. <https://doi.org/10.1093/treephys/20.18.1219>
- Eckenwalder, J. E. (1996). Systematics and evolution of *Populus*. I. In R. F. Stettler, H. D. Bradshaw, P. E. Heilman, & T. M. Hinckley (Eds.), *Biology of Populus and its implications for management and conservation* (pp. 7–32). NRC Research Press.
- Eguchi, N., Morii, N., Ueda, T., Funada, R., Takagi, K., Hiura, T., Sasa, K., & Koike, T. (2008). Changes in petiole hydraulic properties and leaf water flow in birch and oak saplings in a CO₂-enriched atmosphere. *Tree Physiology*, 28(2), 287–295. <https://doi.org/10.1093/treephys/28.2.287>
- Eilmann, B., Zweifel, R., Buchmann, N., Graf Pannatier, E., & Rigling, A. (2011). Drought alters timing, quantity, and quality of wood formation in Scots pine. *Journal of Experimental Botany*, 62(8), 2763–2771. <https://doi.org/10.1093/jxb/erq443>
- Evans, L. M., Kaluthota, S., Pearce, D. W., Allan, G. J., Floate, K., Rood, S. B., & Whitham, T. G. (2016). Bud phenology and growth are subject to divergent selection across a latitudinal gradient in *Populus angustifolia* and impact adaptation across the distributional range and associated arthropods. *Ecology and Evolution*, 6(13), 4565–4581. <https://doi.org/10.1002/ece3.2222>
- Fauset, S., Freitas, H. C., Galbraith, D. R., Sullivan, M. J. P., Aidar, M. P. M., Joly, C. A., Phillips, O. L., Vieira, S. A., & Gloor, M. U. (2018). Differences in leaf thermoregulation and water use strategies between three co-occurring Atlantic forest tree species: Leaf energy balance of Atlantic forest trees. *Plant, Cell & Environment*, 41(7), 1618–1631. <https://doi.org/10.1111/pce.13208>
- Fischer, D. G., Wimp, G. M., Hersch-Green, E., Bangert, R. K., LeRoy, C. J., Bailey, J. K., Schweitzer, J. A., Dirks, C., Hart, S. C., Allan, G. J., & Whitham, T. G. (2017). Tree genetics strongly affect forest productivity, but intraspecific diversity–productivity relationships do not. *Functional Ecology*, 31(2), 520–529. <https://doi.org/10.1111/1365-2435.12733>
- Franks, P. J., & Farquhar, G. D. (2001). The effect of exogenous abscisic acid on stomatal development, stomatal mechanics, and leaf gas exchange in *Tradescantia virginiana*. *Plant Physiology*, 125(2), 935–942. <https://doi.org/10.1104/pp.125.2.935>
- Franks, P. J., & Farquhar, G. D. (2007). The mechanical diversity of stomata and its significance in gas-exchange control. *Plant Physiology*, 143(1), 78–87. <https://doi.org/10.1104/pp.106.089367>
- Freschet, G. T., Cornelissen, J. H. C., van Logtestijn, R. S. P., & Aerts, R. (2010). Evidence of the 'plant economics spectrum' in a subarctic flora. *Journal of Ecology*, 98(2), 362–373. <https://doi.org/10.1111/j.1365-2745.2009.01615.x>

- Friedman, J. M., Roelle, J. E., & Cade, B. S. (2011). Genetic and environmental influences on leaf phenology and cold hardiness of native and introduced riparian trees. *International Journal of Biometeorology*, 55(6), 775–787. <https://doi.org/10.1007/s00484-011-0494-6>
- Garfin, G., Jardine, A., Merideth, R., Black, M., & LeRoy, S. (2013). *Assessment of Climate Change in the Southwest United States*. National Climate Assessment Regional Technical Input Report Series Assessment, (February), 531. <https://doi.org/10.5822/978-1-61091-484-0>
- Gärtner, H., Lucchinetti, S., & Schweingruber, F. H. (2014). New perspectives for wood anatomical analysis in dendrosciences: The GSL1-microtome. *Dendrochronologia*, 32(1), 47–51. <https://doi.org/10.1016/j.dendro.2013.07.002>
- Gazal, R. M., Scott, R. L., Goodrich, D. C., & Williams, D. G. (2006). Controls on transpiration in a semiarid riparian cottonwood forest. *Agricultural and Forest Meteorology*, 137(1–2), 56–67. <https://doi.org/10.1016/j.agrformet.2006.03.002>
- Germino, M. J., Moser, A. M., & Sands, A. R. (2019). Adaptive variation, including local adaptation, requires decades to become evident in common gardens. *Ecological Applications*, 29(2), 1–7. <https://doi.org/10.1002/eap.1842>
- Gleason, S. M., Butler, D. W., Ziemiriska, K., Waryszak, P., & Westoby, M. (2012). Stem xylem conductivity is key to plant water balance across Australian angiosperm species: Plant stem hydraulic traits. *Functional Ecology*, 26(2), 343–352. <https://doi.org/10.1111/j.1365-2435.2012.01962.x>
- Grady, K. C., Ferrier, S. M., Kolb, T. E., Hart, S. C., Allan, G. J., & Whitham, T. G. (2011). Genetic variation in productivity of foundation riparian species at the edge of their distribution: Implications for restoration and assisted migration in a warming climate. *Global Change Biology*, 17(12), 3724–3735. <https://doi.org/10.1111/j.1365-2486.2011.02524.x>
- Grady, K. C., Kolb, T. E., Ikeda, D. H., & Whitham, T. G. (2015). A bridge too far: Cold and pathogen constraints to assisted migration of riparian forests: Assisted migration in riparian restoration. *Restoration Ecology*, 23(6), 811–820. <https://doi.org/10.1111/rec.12245>
- Grady, K. C., Laughlin, D. C., Ferrier, S. M., Kolb, T. E., Hart, S. C., Allan, G. J., & Whitham, T. G. (2013). Conservative leaf economic traits correlate with fast growth of genotypes of a foundation riparian species near the thermal maximum extent of its geographic range. *Functional Ecology*, 27, 427–438. <https://doi.org/10.1111/1365-2435.12060>
- Grossman, G. D., Nickerson, D. M., & Freeman, M. C. (1991). Principal component analyses of assemblage structure data: Utility of tests based on eigenvalues. *Ecology*, 72(1), 341–347. <https://doi.org/10.2307/1938927>
- Hacke, U. G., Sperry, J. S., & Pittermann, J. (2000). Drought experience and cavitation resistance in six shrubs from the Great Basin, Utah. *Basic and Applied Ecology*, 1(1), 31–41. <https://doi.org/10.1078/1439-1791-00006>
- Hacke, U. G., Sperry, J. S., Pockman, W. T., Davis, S. D., & McCulloh, K. A. (2001). Trends in wood density and structure are linked to prevention of xylem implosion by negative pressure. *Oecologia*, 126(4), 457–461. <https://doi.org/10.1007/s004420100628>
- Hajek, P., Leuschner, C., Hertel, D., Delzon, S., & Schuldt, B. (2014). Trade-offs between xylem hydraulic properties, wood anatomy and yield in *Populus*. *Tree Physiology*, 34(7), 744–756. <https://doi.org/10.1093/treephys/tpu048>
- Haworth, M., Belcher, C. M., Killi, D., Dewhurst, R. A., Materassi, A., Raschi, A., & Centritto, M. (2018). Impaired photosynthesis and increased leaf construction costs may induce floral stress during episodes of global warming over macroevolutionary timescales. *Scientific Reports*, 8(1), 6206. <https://doi.org/10.1038/s41598-018-24459-z>
- Hetherington, A. M., & Woodward, F. I. (2003). The role of stomata in sensing and driving environmental change. *Nature*, 424(6951), 901–908. <https://doi.org/10.1038/nature01843>
- Hilu, K. W., & Randall, J. L. (1984). Convenient method for studying grass leaf epidermis. *Taxon*, 33(3), 413. <https://doi.org/10.2307/1220980>
- Hultine, K. R., Allan, G. J., Blasini, D., Bothwell, H. M., Cadmus, A., Cooper, H. F., Doughty, C. E., Gehring, C. A., Gitlin, A. R., Grady, K. C., Hull, J. B., Keith, A. R., Koepke, D. F., Markovchick, L., Corbin Parker, J. M., Sankey, T. T., & Whitham, T. G. (2020). Adaptive capacity in the foundation tree species *Populus fremontii*: Implications for resilience to climate change and non-native species invasion in the American Southwest. *Conservation Physiology*, 8(1). <https://doi.org/10.1093/conphys/coaa061>
- Hultine, K. R., Burtch, K. G., & Ehleringer, J. R. (2013). Gender specific patterns of carbon uptake and water use in a dominant riparian tree species exposed to a warming climate. *Global Change Biology*, 19(11), 3390–3405. <https://doi.org/10.1111/gcb.12230>
- Hultine, K. R., & Bush, S. E. (2011). Ecohydrological consequences of non-native riparian vegetation in the southwestern United States: A review from an ecophysiological perspective: Non-native species impacts on riparian ecohydrology. *Water Resources Research*, 47(7). <https://doi.org/10.1029/2010WR010317>
- Hultine, K. R., Bush, S. E., & Ehleringer, J. R. (2010). Ecophysiology of riparian cottonwood and willow before, during, and after two years of soil water removal. *Ecological Applications*, 20(2), 347–361. <https://doi.org/10.1890/09-0492.1>
- Hultine, K. R., Froend, R., Blasini, D., Bush, S. E., Karlinski, M., & Koepke, D. F. (2020). Hydraulic traits that buffer deep-rooted plants from changes in hydrology and climate. *Hydrological Processes*, 34(2), 209–222. <https://doi.org/10.1002/hyp.13587>
- Ikeda, D. H., Bothwell, H. M., Lau, M. K., O'Neill, G. A., Grady, K. C., & Whitham, T. G. (2014). A genetics-based Universal Community Transfer Function for predicting the impacts of climate change on future communities. *Functional Ecology*, 28(1), 65–74. <https://doi.org/10.1111/1365-2435.12151>
- Ikeda, D. H., Max, T. L., Allan, G. J., Lau, M. K., Shuster, S. M., & Whitham, T. G. (2017). Genetically informed ecological niche models improve climate change predictions. *Global Change Biology*, 23, 164–176. <https://doi.org/10.1111/gcb.13470>
- Jackson, D. A. (1993). Stopping rules in principal components analysis: A comparison of heuristic and statistical approaches. *Ecology*, 74(8), 2204–2214. <https://doi.org/10.2307/1939574>
- Jones, D. A., O'Hara, K. L., Battles, J. J., & Gersonde, R. F. (2015). Leaf area prediction using three alternative sampling methods for seven Sierra Nevada conifer species. *Forests*, 6(8), 2631–2654. <https://doi.org/10.3390/f6082631>
- Jones, H. G. (2013). *Plants and microclimate: A quantitative approach to environmental plant physiology* (3rd ed.). Cambridge University Press. <https://doi.org/10.1017/CBO9780511845727>
- Joshua Leffler, A., England, L. E., & Naito, J. (2000). Vulnerability of Fremont cottonwood (*Populus fremontii* Wats.) individuals to xylem cavitation. *Western North American Naturalist*. Retrieved from <https://scholarsarchive.byu.edu/wnan/vol60/iss2/10>
- Kassambara, A., & Mundt, F. (2017). factoextra: Extract and visualize the results of multivariate data analyses. R package version 1.0.5. <https://CRAN.Rproject.org/package=factoextra>
- Kawecki, T. J., & Ebert, D. (2004). Conceptual issues in local adaptation. *Ecology Letters*, 7(12), 1225–1241. <https://doi.org/10.1111/j.1461-0248.2004.00684.x>
- Kenefic, L. S., & Seymour, R. S. (1999). Leaf area prediction models for *Tsuga canadensis* in Maine. *Canadian Journal of Forest Research*, 29(10), 1574–1582. <https://doi.org/10.1139/x99-134>
- Kleyer, M., & Minden, V. (2015). Why functional ecology should consider all plant organs: An allocation-based perspective. *Basic and Applied Ecology*, 16(1), 1–9. <https://doi.org/10.1016/j.baae.2014.11.002>
- Kolb, K. J., & Sperry, J. S. (1999). Differences in drought adaptation between subspecies of sagebrush (*Artemisia tridentata*). *Ecology*, 80(7), 2373–2384. <https://doi.org/10.2307/176917>
- Körner, C. (2003). *Alpine plant life: Functional plant ecology of high mountain ecosystems* (2nd ed.). Springer.

- Kuznetsova, A., Brockhoff, P. B., & Christensen, R. H. B. (2017). lmerTest package: Tests in linear mixed effects models. *Journal of Statistical Software*, 82(13). <https://doi.org/10.18637/jss.v082.i13>
- Lambers, H., Chapin, F. S., & Pons, T. L. (1998). Photosynthesis, respiration, and long-distance transport. In *Plant physiological ecology* (pp. 10–153). https://doi.org/10.1007/978-1-4757-2855-2_2
- Lambers, H., Chapin, F. S., & Pons, T. L. (2008). *Plant physiological ecology*. Springer. <https://doi.org/10.1007/978-0-387-78341-3>
- Lambers, H., & Poorter, H. (1992). Inherent variation in growth rate between higher plants: A search for physiological causes and ecological consequences. *Advances in Ecological Research*, 23(C), 187–261. [https://doi.org/10.1016/S0065-2504\(08\)60148-8](https://doi.org/10.1016/S0065-2504(08)60148-8)
- Lauri, P. (2019). Corner's rules as a framework for plant morphology, architecture and functioning – Issues and steps forward. *New Phytologist*, 221(4), 1679–1684. <https://doi.org/10.1111/nph.15503>
- Lê, S., Josse, J., & Husson, F. (2008). FactoMineR: An R package for multivariate analysis. *Journal of Statistical Software*, 25(1). <https://doi.org/10.18637/jss.v025.i01>
- Li, Y., Sperry, J. S., Taneda, H., Bush, S. E., & Hacke, U. G. (2008). Evaluation of centrifugal methods for measuring xylem cavitation in conifers, diffuse- and ring-porous angiosperms. *New Phytologist*, 177(2), 558–568. <https://doi.org/10.1111/j.1469-8137.2007.02272.x>
- Lindtke, D., González-Martínez, S. C., Macaya-Sanz, D., & Lexer, C. (2013). Admixture mapping of quantitative traits in *Populus* hybrid zones: Power and limitations. *Heredity*, 111(6), 474–485. <https://doi.org/10.1038/hdy.2013.69>
- Mayr, S., Schmid, P., Laur, J., Rosner, S., Charra-Vaskou, K., Dämon, B., & Hacke, U. G. (2014). Uptake of water via branches helps timberline conifers refill embolized xylem in late winter. *Plant Physiology*, 164(4), 1731–1740. <https://doi.org/10.1104/pp.114.236646>
- Mayr, S., & Sperry, J. S. (2010). Freeze-thaw-induced embolism in *Pinus contorta*: Centrifuge experiments validate the 'thaw-expansion hypothesis' but conflict with ultrasonic emission data. *New Phytologist*, 185(4), 1016–1024. <https://doi.org/10.1111/j.1469-8137.2009.03133.x>
- Merriitt, D. M., & Leroy Poff, N. (2010). Shifting dominance of riparian *Populus* and *Tamarix* along gradients of flow alteration in western North American rivers. *Ecological Applications*, 20(1), 135–152. <https://doi.org/10.1890/08-2251.1>
- Messier, J., Lechowicz, M. J., McGill, B. J., Violle, C., & Enquist, B. J. (2017). Interspecific integration of trait dimensions at local scales: The plant phenotype as an integrated network. *Journal of Ecology*, 105(6), 1775–1790. <https://doi.org/10.1111/1365-2745.12755>
- Michaletz, S. T., Weiser, M. D., Zhou, J., Kaspari, M., Helliker, B. R., & Enquist, B. J. (2015). Plant thermoregulation: Energetics, trait-environment interactions, and carbon economics. *Trends in Ecology & Evolution*, 30(12), 714–724. <https://doi.org/10.1016/j.tree.2015.09.006>
- Mooney, H. A., & Billings, W. D. (1961). Comparative physiological ecology of arctic and alpine populations of *Oxyria digyna*. *Ecological Monographs*, 31(1), 1–29. <https://doi.org/10.2307/1950744>
- Niklas, K. J. (1991). Flexural stiffness allometries of angiosperm and fern petioles and rachises: Evidence for biomechanical convergence. *Evolution*, 45(3), 734. <https://doi.org/10.2307/2409924>
- Niklas, K. J., & Spatz, H.-C. (2010). Worldwide correlations of mechanical properties and green wood density. *American Journal of Botany*, 97(10), 1587–1594. <https://doi.org/10.3732/ajb.1000150>
- Niklas, K. J., & Spatz, H.-C. (2012). Mechanical properties of wood disproportionately increase with increasing density. *American Journal of Botany*, 99(1), 169–170. <https://doi.org/10.3732/ajb.1100567>
- Nobel, P. S. (2009). *Physicochemical and environmental plant physiology* (4th ed.). Elsevier/Academic Press. <https://doi.org/10.1016/B978-0-12-374143-1.X0001-4>
- O'Grady, A. P., Cook, P. G., Eamus, D., Duguid, A., Wischusen, J. D. H., Fass, T., & Worldege, D. (2009). Convergence of tree water use within an arid-zone woodland. *Oecologia*, 160(4), 643–655. <https://doi.org/10.1007/s00442-009-1332-y>
- O'Neill, G. A., Hamann, A., & Wang, T. (2008). Accounting for population variation improves estimates of the impact of climate change on species growth and distribution. *Journal of Applied Ecology*, 45(4), 1040–1049. <https://doi.org/10.1111/j.1365-2664.2008.01472.x>
- O'Sullivan, O. S., Heskell, M. A., Reich, P. B., Tjoelker, M. G., Weerasinghe, L. K., Penillard, A., Zhu, L., Egerton, J. J. G., Bloomfield, K. J., Creek, D., Bahar, N. H. A., Griffin, K. L., Hurry, V., Meir, P., Turnbull, M. H., & Atkin, O. K. (2017). Thermal limits of leaf metabolism across biomes. *Global Change Biology*, 23(1), 209–223. <https://doi.org/10.1111/gcb.13477>
- Pásztor, Z., & Ronyecz, I. (2013). The thermal insulation capacity of tree bark. *Acta Silvatica et Lignaria Hungarica*, 9(1), 111–117. <https://doi.org/10.2478/aslh-2013-0009>
- Peres-Neto, P. R., Jackson, D. A., & Somers, K. M. (2005). How many principal components? Stopping rules for determining the number of non-trivial axes revisited. *Computational Statistics and Data Analysis*, 49(4), 974–997. <https://doi.org/10.1016/j.csda.2004.06.015>
- Preibisch, S., Saalfeld, S., & Tomancak, P. (2009). Globally optimal stitching of tiled 3D microscopic image acquisitions. *Bioinformatics*, 25(11), 1463–1465. <https://doi.org/10.1093/bioinformatics/btp184>
- Preston, K. A., Cornwell, W. K., & DeNoyer, J. L. (2006). Wood density and vessel traits as distinct correlates of ecological strategy in 51 California coast range angiosperms. *New Phytologist*, 170(4), 807–818. <https://doi.org/10.1111/j.1469-8137.2006.01712.x>
- R Core Team. (2019). *R: A language and environment for statistical computing*. R Foundation Statistical Computing. Retrieved from <https://www.r-project.org/>
- Ravikumar, S., Surekha, R., & Thavarajah, R. (2014). Mounting media: An overview. *Journal of Dr. NTR University of Health Sciences*, 3(5), 1. <https://doi.org/10.4103/2277-8632.128479>
- Reich, P. B. (2014). The world-wide 'fast-slow' plant economics spectrum: A traits manifesto. *Journal of Ecology*, 102(2), 275–301. <https://doi.org/10.1111/1365-2745.12211>
- Reich, P. B., Wright, I. J., Cavender-Bares, J., Craine, J. M., Oleksyn, J., Westoby, M., & Walters, M. B. (2003). The evolution of plant functional variation: Traits, spectra, and strategies. *International Journal of Plant Sciences*, 164(S3), S143–S164. <https://doi.org/10.1086/374368>
- Roden, J. S., & Pearcy, R. W. (1993). Effect of leaf flutter on the light environment of poplars. *Oecologia*, 93(2), 201–207. <https://doi.org/10.1007/BF00317672>
- Rosas, T., Mencuccini, M., Barba, J., Cochard, H., Saura-Mas, S., & Martínez-Vilalta, J. (2019). Adjustments and coordination of hydraulic, leaf and stem traits along a water availability gradient. *New Phytologist*, 223(2), 632–646. <https://doi.org/10.1111/nph.15684>
- Rosell, J. A. (2016). Bark thickness across the angiosperms: More than just fire. *New Phytologist*, 211(1), 90–102. <https://doi.org/10.1111/nph.13889>
- Rueda, M., Godoy, O., & Hawkins, B. A. (2018). Trait syndromes among North American trees are evolutionarily conserved and show adaptive value over broad geographic scales. *Ecography*, 41(3), 540–550. <https://doi.org/10.1111/ecog.03008>
- Sack, L., Cowan, P. D., Jaikumar, N., & Holbrook, N. M. (2003). The 'hydrology' of leaves: Co-ordination of structure and function in temperate woody species. *Plant, Cell and Environment*, 26(8), 1343–1356. <https://doi.org/10.1046/j.0016-8025.2003.01058.x>
- Sack, L., & Frolé, K. (2006). Leaf structural diversity is related to hydraulic capacity in tropical rain forest trees. *Ecology*, 87(2), 483–491. <https://doi.org/10.1890/05-0710>
- Scholander, P. F., Bradstreet, E. D., Hemmingsen, E. A., & Hammel, H. T. (1965). Sap pressure in vascular plants: Negative hydrostatic pressure can be measured in plants. *Science*, 148(3668), 339–346. <https://doi.org/10.1126/science.148.3668.339>

- Scholz, A., Klepsch, M., Karimi, Z., & Jansen, S. (2013). How to quantify conduits in wood? *Frontiers in Plant Science*, 4, 1–11. <https://doi.org/10.3389/fpls.2013.00056>
- Sharkey, T. D. (2005). Effects of moderate heat stress on photosynthesis: Importance of thylakoid reactions, rubisco deactivation, reactive oxygen species, and thermotolerance provided by isoprene. *Plant, Cell and Environment*, 28(3), 269–277. <https://doi.org/10.1111/j.1365-3040.2005.01324.x>
- Smith, D. M., & Allen, S. J. (1996). Measurement of sap flow in plant stems. *Journal of Experimental Botany*, 47(305), 1833–1844. <https://doi.org/10.1093/jxb/47.12.1833>
- Sokal, R. R., & Rohlf, F. J. (1995). *Biometry: The principles and practice of statistics in biological research* (3rd ed.). W.H. Freeman.
- Sperry, J. S., & Saliendra, N. Z. (1994). Intra- and inter-plant variation in xylem cavitation in *Betula occidentalis*. *Plant, Cell and Environment*, 17(11), 1233–1241. <https://doi.org/10.1111/j.1365-3040.1994.tb02021.x>
- Sperry, J. S., & Sullivan, J. E. M. (1992). Xylem embolism in response to freeze-thaw cycles and water stress in ring-porous, diffuse-porous, and conifer species. *Plant Physiology*, 100(2), 605–613. <https://doi.org/10.1104/pp.100.2.605>
- Sprugel, D. G. (1989). The relationship of evergreenness, crown architecture, and leaf size. *The American Naturalist*, 133(4), 465–479. <https://doi.org/10.1086/284930>
- Sridharan, G., & Shankar, A. A. (2012). Toluidine blue: A review of its chemistry and clinical utility. *Journal of Oral and Maxillofacial Pathology*, 16(2), 251–255. <https://doi.org/10.4103/0973-029X.99081>
- Sterck, F. J., Zweifel, R., Sass-Klaassen, U., & Chowdhury, Q. (2008). Persisting soil drought reduces leaf specific conductivity in Scots pine (*Pinus sylvestris*) and pubescent oak (*Quercus pubescens*). *Tree Physiology*, 28(4), 529–536. <https://doi.org/10.1093/treephys/28.4.529>
- Stromberg, J. C. (1993). Frémont cottonwood-Goodding willow riparian forests: A review of their ecology, threats, and recovery potential. *Journal of the Arizona-Nevada Academy of Sciences*, 26(3), 97–110.
- Trueba, S., Isnard, S., Barthélémy, D., & Olson, M. E. (2016). Trait coordination, mechanical behaviour and growth form plasticity of *Amborella trichopoda* under variation in canopy openness. *AoB PLANTS*, 8, plw068. <https://doi.org/10.1093/aobpla/plw068>
- Tyree, M. E., & Zimmermann, M. H. (2002). *Xylem Structure and the ascent of sap* (2nd edn.). Springer Verlag.
- Valladares, F., Skillman, J. B., & Pearcy, R. W. (2002). Convergence in light capture efficiencies among tropical forest understory plants with contrasting crown architectures: A case of morphological compensation. *American Journal of Botany*, 89(8), 1275–1284. <https://doi.org/10.3732/ajb.89.8.1275>
- Wang, T., Hamann, A., Spittlehouse, D. L., & Murdock, T. Q. (2012). ClimateWNA-high-resolution spatial climate data for western North America. *Journal of Applied Meteorology and Climatology*, 51(1), 16–29. <https://doi.org/10.1175/JAMC-D-11-043.1>
- Whitham, T. G., DiFazio, S. P., Scheitzer, J. A., Shuster, S. M., Allan, G. J., Bailey, J. K., & Woolbright, S. A. (2008). Extending genomics to natural communities and ecosystems. *Science*, 320, 492–495. <https://doi.org/10.1126/science.1153918>
- Williams, A. P., Cook, E. R., Smerdon, J. E., Cook, B. I., Abatzoglou, J. T., Bolles, K., Baek, S. H., Badger, A. M., & Livneh, B. (2020). Large contribution from anthropogenic warming to an emerging North American megadrought. *Science*, 368(6488), 314–318. <https://doi.org/10.1126/science.aaz9600>
- Worrall, J. J., Egeland, L., Eager, T., Mask, R. A., Johnson, E. W., Kemp, P. A., & Sheppard, W. D. (2008). Rapid mortality of *Populus tremuloides* in southwestern Colorado, USA. *Forest Ecology and Management*, 255(3), 686–696. <https://doi.org/10.1016/j.foreco.2007.09.071>
- Worrall, J. J., Rehfeldt, G. E., Hamann, A., Hogg, E. H., Marchetti, S. B., Michaelin, M., & Gray, L. K. (2013). Recent declines of *Populus tremuloides* in North America linked to climate. *Forest Ecology and Management*, 299, 35–51. <https://doi.org/10.1016/j.foreco.2012.12.033>
- Wright, I. J., Reich, P. B., Westoby, M., Ackerly, D. D., Baruch, Z., Bongers, F., Cavender-Bares, J., Chapin, T., Cornelissen, J. H. C., Diemer, M., Flexas, J., Garnier, E., Groom, P. K., Gulias, J., Hikosaka, K., Lamont, B. B., Lee, T., Lee, W., Lusk, C., ... Villar, R. (2004). The worldwide leaf economics spectrum. *Nature*, 428(6985), 821–827. <https://doi.org/10.1038/nature02403>
- Wright, I. J., & Westoby, M. (2002). Leaves at low versus high rainfall: Coordination of structure, lifespan and physiology. *New Phytologist*, 155(3), 403–416. <https://doi.org/10.1046/j.1469-8137.2002.00479.x>
- Zaehle, S. (2005). Effect of height on tree hydraulic conductance incompletely compensated by xylem tapering. *Functional Ecology*, 19(2), 359–364. <https://doi.org/10.1111/j.0269-8463.2005.00953.x>
- Zhou, H., Chen, Y., Zhu, C., Li, Z., Fang, G., Li, Y., & Fu, A. (2020). Climate change may accelerate the decline of desert riparian forest in the lower Tarim River, northwestern China: Evidence from tree-rings of *Populus euphratica*. *Ecological Indicators*, 111, 105997. <https://doi.org/10.1016/j.ecolind.2019.105997>
- Zweifel, R., & Häsler, R. (2000). Frost-induced reversible shrinkage of bark of mature subalpine conifers. *Agricultural and Forest Meteorology*, 102(4), 213–222. [https://doi.org/10.1016/S0168-1923\(00\)00135-0](https://doi.org/10.1016/S0168-1923(00)00135-0)

SUPPORTING INFORMATION

Additional supporting information may be found online in the Supporting Information section.

How to cite this article: Blasini DE, Koepke DF, Grady KC, et al. Adaptive trait syndromes along multiple economic spectra define cold and warm adapted ecotypes in a widely distributed foundation tree species. *J Ecol.* 2020;00:1–21. <https://doi.org/10.1111/1365-2745.13557>